

Tuuli Lehti

Effects of Deep Brain Stimulation on Corticomuscular and Corticokinematic Coherence in Advanced Parkinson's Disease

Department of Electrical Engineering and Automation

Thesis submitted for examination for the degree of Master of Science in Technology.

Helsinki 21.5.2014

Supervisor:

Prof. Tomi Laurila

Thesis instructors:

M.Sc. Liisa Helle

D.Sc. Emilia Kaivosoja

Tekijä: Tuuli Lehti

Työn nimi: Syväaivostimulaation vaikutus kortikomuskulaariseen ja kortikokinemaattiseen koherenssiin pitkälle edenneessä Parkinsonin taudissa

Päivämäärä: 21.5.2014

Kieli: Englanti

Sivumäärä: 8+59

Sähkötekniikan ja automaation laitos

Professuuri: Mikrosysteemitekniikka

Koodi: S-113

Valvoja: Prof. Tomi Laurila

Ohjaajat: DI Liisa Helle, TkT Emilia Kaivosoja

Rytmissen aktiivisuuden tahdistuminen eri aivoalueiden välillä kertoo niiden välisestä kommunikaatiosta ja on edellytys aivojen toiminnalle. Liikeaivokuoren ja supistuvan lihaksen välinen tahdistuminen on samoin onnistuneen liikesäätelyn edellytys. Parkinsonin taudissa on havaittu poikkeavuuksia sekä aivokuoren rytmisessä toiminnassa että lihaksen ja aivokuoren välisessä tahdistumisessa erityisesti taajuusvälillä 14–30 Hz. Aivokuoren ja lihaksen välistä tahdistumista voidaan mitata kortikomuskulaarisen koherenssin avulla ei-invasiivisesti käyttämällä magnetoenkefalografia- (MEG) ja elektromyografi mittauksia (EMG).

Pitkälle edenneen Parkinsonin taudin oireita voidaan lievittää syväaivostimulaatiolla (DBS). Vaikka DBS:n tiedetään voivan lievittää oireita lääkehoitoakin paremmin, sen vaikutusmekanismi on epäselvä. Tämän työn keskeinen tavoite oli valaista DBS:n vaikutusta kortikomuskulaariseen koherenssiin Parkinson-potilailla. Lisäksi kortikomuskulaarisen koherenssin fysiologista merkitystä tutkittiin vertaamalla sitä etusormen asentovapinaan ranteen staattisen koukistuksen aikana. Tätä varten kortikomuskulaarista koherenssia verrattiin kortikokinemaattiseen koherenssiin, joka kuvaa MEG-signaalin ja sormen vapinan välistä tahdistumista. Koherenttien lähteiden paikannukseen käytettiin beamformer-menetelmää. Tutkimukseen kuului kolme DBS-potilasta, joilla oli pitkälle edennyt Parkinsonin tauti, ja kymmenen tervettä kontrollia.

Havaitsimme lievää asentovapinaa kaikilla potilailla (5–7 Hz) ja yhdeksällä kymmenestä kontrollista (8–11 Hz). Kaikilla koehenkilöillä oli tilastollisesti merkittävää kortikomuskulaarista ja -kinemaattista koherenssia välillä 14–30 Hz, ja koherenssimaksimit paikantuivat vastakkaisen aivopuoliskon sensorimotoriselle aivokuorelle sekä potilailla että kontrolleilla. Kahdella kolmesta potilaasta koherenssin voimakkuus kasvoi, kun DBS oli kytketty pois; kasvu korreloi positiivisesti kliinisten oireiden pahenemisen kanssa. Kolmannella potilaalla koherenssi aleni stimulaation poiskytkemisen jälkeen, mutta samalla oireet hieman helpottuivat. Tämä on ensimmäinen tutkimus, joka mittaa kortikokinemaattista koherenssia kortikomuskulaarisen koherenssin yhteydessä Parkinson-potilailla.

Avainsanat: Parkinsonin tauti, syväaivostimulaatio, magnetoenkefalografia, kortikomuskulaarinen koherenssi, kortikokinemaattinen koherenssi

Author: Tuuli Lehti

Title: Effects of Deep Brain Stimulation on Corticomuscular and
Corticokinematic Coherence in Advanced Parkinson's Disease

Date: 21.5.2014

Language: English

Number of pages:8+59

Department of Electrical Engineering and Automation

Professorship: Microsystems technology

Code: S-113

Supervisor: Prof. Tomi Laurila

Instructors: M.Sc. Liisa Helle, D.Sc. Emilia Kaivosoja

Regions of the brain exhibit characteristic oscillatory firing patterns. Synchronous oscillations between distinct regions reflect connectivity and are considered necessary for the proper functioning of the brain. Similarly, synchrony between the motor cortex and a contracting muscle is necessary for motor control. The motor disability observed in Parkinson's disease (PD) has been associated with alterations in cortical oscillations and brain-muscle synchrony at the beta band (14–30 Hz). Brain-muscle synchrony can be quantified as corticomuscular coherence (CMC) that can be measured noninvasively using magnetoencephalography (MEG) and electromyography (EMG).

A patient with advanced PD may benefit from high-frequency stimulation of the subthalamic nucleus (STN). Although deep brain stimulation (DBS) offers benefits superior to best available medical therapy, its mechanism of action remains poorly understood. A central aim of this Thesis was to elucidate the effects of DBS on CMC in patients with PD. Another aim was to clarify the physiological relevance of CMC by relating it to limb kinematics. To that end, we compared CMC with corticokinematic coherence (CKC) that quantifies synchrony between MEG and the small-amplitude postural tremor of the hand during static wrist extension. To localize the coherent sources in the brain, we employed beamforming. We measured CMC and CKC in three patients with advanced PD and in ten healthy controls. All patients were using bilateral DBS.

We observed small-amplitude postural tremor in all patients (5–7 Hz) and in nine out of ten controls (8–11 Hz). All subjects had statistically significant CMC and CKC at the beta band; the CMC and CKC maxima colocalized at the sensorimotor cortex contralateral to the task-performing hand both in patients and in healthy controls. Two out of three patients had stronger coherence with DBS off than with DBS on, and the change correlated with the worsening of motor symptoms. The third patient had lower coherence with DBS off but simultaneously showed a mild improvement in motor symptoms when the stimulation had been switched off. This is the first study to measure CKC in unison with CMC in patients with PD.

Keywords: Parkinson's disease, deep brain stimulation, magnetoencephalography, corticomuscular coherence, corticokinematic coherence

Preface

Many people have contributed to this Thesis project over the past year. First of all, I wish to thank my instructors, D.Sc. Emilia Kaivosoja and M.Sc. Liisa Helle, for their support, inspirational efficiency, and intelligent advice, and my supervisor Prof. Tomi Laurila for his fresh take on things and the open-mindedness that made this project possible to begin with.

Great thanks go to Docent Jyrki Mäkelä and M.D., Ph.D. Eero Pekkonen for providing me with a Thesis project at the BioMag Laboratory: thank you, Eero, for saying yes without a moment's hesitation, and thank you, Jyrki, for your scientific vision and for the patient encouragement throughout the process. My deepest thanks equally belong to M.D. Katja Airaksinen, who had collected the data and who provided me with well-chosen literature and some greatly appreciated peer support.

The people of BioMag have supported me enormously, and I wish to thank everyone involved: M.Sc. Juha Montonen, a man of admirable calm, D.Sc. Pantelis Lioumis, my intellectual adviser and life-coach in disguise, Pirjo Kari, the heart and soul of BioMag, and all others. Special thanks go to M.Sc. Jarkko Luoma and soon-to-be Ph.D. Jussi Nurminen, my tireless technical, scientific and life-philosophical supporters. Thank you for having the patience to compensate for my lack of it.

Friends near and far have played important parts in bringing me where I stand now. I thank my medical school teammates in R7 Team Viima and Musatiimi, and the wonderful people of FiestaFlamenca for the inspiration and the fun. I thank my parents for having raised me astonishingly free of expectations and my brother for reminding me of the power of a free spirit.

Helsinki, 21.5.2014

Tuuli Elina Lehti

Contents

Abstract (in Finnish)	ii
Abstract	iii
Preface	iv
1 Introduction	1
2 Theory	3
2.1 Parkinson's disease	3
2.1.1 Clinical features	3
2.1.2 Pathophysiology	4
2.2 Deep brain stimulation	7
2.2.1 Patient selection	7
2.2.2 Instrumentation and surgical procedure	8
2.2.3 Effect on physiology	10
2.3 Magnetoencephalography (MEG)	11
2.3.1 Neural correlates of MEG	12
2.3.2 Instrumentation	13
2.3.3 Interference suppression	15
2.3.4 Source modeling	19
2.4 Coherence	22
2.4.1 Magnitude squared coherence	23
2.4.2 Corticomuscular coherence	23
2.4.3 Corticomuscular coherence in Parkinson's disease	24
2.4.4 Corticokinematic coherence	25
3 Materials and methods	27
3.1 Subjects	27
3.2 Experimental protocol	27
3.3 Data collection	29
3.3.1 MEG and MRI data collection	29
3.3.2 Phantom measurements	29
3.4 Data preprocessing	29

3.4.1	Artefact identification	29
3.4.2	Coregistration and MRI preprocessing	31
3.4.3	MEG data preprocessing	33
3.5	Data analysis	33
3.5.1	Spectrum analysis	33
3.5.2	Sensor-level coherence	33
3.5.3	Source-space coherence	34
4	Results	35
4.1	Motor disability scores (UPDRS III)	35
4.2	Spectrum analysis	35
4.3	Sensor-level coherence	37
4.4	Source-space coherence	39
5	Discussion	43
6	Conclusion	46
	References	47
	Appendices	54
A	Patients: power spectra	54
B	Controls: coherence maxima	57

Abbreviations

CKC	corticokinematic coherence
CMC	corticomuscular coherence
DBS	deep brain stimulation
EEG	electroencephalography
EMG	electromyography
GPe	globus pallidus externa
GPi	globus pallidus interna
HPI	head position indicator
MEG	magnetoencephalography
MRI	magnetic resonance image
PD	Parkinson's disease
SNc	substantia nigra pars compacta
SNr	substantia nigra pars reticulata
SQUID	superconducting quantum interference device
STN	subthalamic nucleus
SSS	signal space separation
tSSS	spatiotemporal signal space separation
UPDRS	Unified Parkinson's Disease Rating Scale

Symbols

\mathbf{A}	data covariance matrix
\mathbf{B}	magnetic field
C_{xy}	coherence between signals a and b
f	frequency
Φ_0	flux quantum
\mathbf{G}	cross-spectral density matrix
G_{aa}	autospectral density (signal a)
G_{ab}	cross-spectral density for signals a and b
\mathbf{h}	forward model projection vector
I_b	feedback current
\mathbf{J}	current density
N	number of samples
N_s	number of sensors
\mathbf{p}	virtual electrode (frequency domain)
\mathbf{q}	virtual electrode (time domain)
r	distance from the origin of the series expansion
V	voltage
ν	modified vector harmonic function
ω	modified vector harmonic function
\mathbf{w}	beamformer weight vector
\mathbf{X}	MEG sensor data matrix
\mathbf{y}	source signal

Vocabulary related to Parkinson's disease

<i>aetiology</i>	the cause of a disease
<i>akinesia</i>	absence of movement, inability to initiate movement
<i>bradykinesia</i>	abnormal slowness of movement
<i>dyskinesia</i>	uncontrolled, involuntary movement
<i>hypokinesia</i>	decrease in movements
<i>idiopathic</i>	primary, arising spontaneously or from unknown cause
<i>levodopa</i>	a dopamine precursor used in standard pharmacotherapy for PD
<i>off state</i>	a phase during which medication fails to mask the symptoms
<i>on state</i>	a phase marked by good response to medication
<i>pathology</i>	the anatomic and functional deviations observed in a disease
<i>pathophysiology</i>	the changes in physiology accompanying a disease
<i>postural</i>	relating to body position or the position of a limb
<i>rigidity</i>	abnormally increased muscle tone

1 Introduction

Parkinson’s disease (PD) is the second most common neurodegenerative disease in Western populations [1]. The classical triad of symptoms consists of tremor, bradykinesia and rigidity¹ and is accompanied by a variety of motor and nonmotor symptoms that impair daily functioning and quality of life. The main hallmark of PD pathology is the gradual degeneration of dopamine-secreting neurons in the subthalamic structure *substantia nigra* that projects to a set of subcortical nuclei collectively known as the basal ganglia. Through connections to the motor cortex, the basal ganglia constitute a complex circuit essential for the regulation of voluntary movements.

Traditional treatments for PD aim at restoring the dopamine supply of the basal ganglia: the gold standard for treatment is levodopa [2], a dopamine precursor that is converted to dopamine in the brain. However, prolonged use of levodopa predisposes the patient to side-effects, such as the wearing-off of drug efficacy and the appearance of involuntary movements, dyskinesias. A novel treatment modality emerged in the 1980s when high-frequency stimulation of subcortical structures was observed to alleviate PD symptoms [3]. Deep brain stimulation (DBS) has now been shown to offer clinical benefits superior to the best available medical therapy for advanced PD [4]. The treatment does not revert disease progression, but the clinical effect persists up to 10 years [5, 6].

The fact that DBS alleviates PD symptoms has reoriented theories on PD pathophysiology towards a view that considers the dynamic nature of neural communication. It has long been known that brain areas exhibit characteristic oscillations traditionally divided into bands by frequency. For example, oscillations around 10 Hz have been classified as alpha activity and those around 20 Hz as beta activity. Here, we define the beta band as the band between 14 and 30 Hz [7]. Excessive beta band oscillations at the level of the basal ganglia have been reported in PD that are decreased after the administration of levodopa [8]. Similarly, clinically effective DBS has been associated with reduced beta activity in the subthalamic nucleus (STN) [9].

The basal ganglia are intimately connected with the motor areas of the cerebral cortex, in particular, the primary motor cortex, which lies anterior to the central sulcus in the posterior frontal lobe. Cortical beta activity was associated with motor function by Penfield in 1954 [10]: he showed that in preparation of a voluntary movement beta activity was attenuated but reappeared with sustained muscle contraction. Recently, it has been shown that this sequence of beta desynchronization and resynchronization is impaired in PD [11].

Conway et al. [12] demonstrated in 1995 that cortical signaling during sustained muscle contraction was coherent with electromyography (EMG) obtained in the contracting muscle. The coherence frequency varied individually but was contained within the beta band. Conway et al. recorded cortical activity with magnetoencephalography (MEG), a highly sensitive measuring modality capable of sensing

¹Medical terminology is explained on page viii.

extremely weak magnetic fields, and thereby coined the term MEG-EMG coherence to describe their finding. Later, the name corticomuscular coherence (CMC) has become established in the field to describe coherence measured between a cortical signal and EMG.

To examine whether CMC could be used as a marker for motor function in PD, Salenius et al. [13] studied eight patients withdrawn from antiparkinsonian medication. They showed that fewer patients had significant beta band CMC when withdrawn from medication than after receiving it. Again, large individual variation was seen in the results. Since then, researchers have slowly begun to adopt CMC as a potential measure for motor function and treatment efficacy in PD.

The study of MEG-EMG coherence in PD patients with DBS is particularly challenging due to the interference caused by the DBS hardware and the stimulation itself. Thanks to recent developments in the computational processing of MEG data, it has now become possible to manage DBS-contaminated data. A method called temporal signal space separation (tSSS) [14] has proven particularly effective in suppressing the interference.

The mechanism through which DBS produces favorable clinical effects still remains poorly understood. This Thesis aims to elucidate the effects of DBS on cortical oscillations by measuring CMC in PD patients with DBS on and off: (i) to examine the physiological role of CMC and its potential involvement in tremor-generation, we correlate CMC with simultaneously measured corticokinematic coherence (CKC) calculated between MEG and the slight postural tremor of the hand; (ii) by using a source estimation method called beamforming we estimate the CMC and CKC source locations and see if the two are colocalized; (iii) finally, we compare the results obtained in patients with those obtained in healthy controls. This is the first study to have looked at both CMC and CKC during static muscle contraction in healthy subjects and in PD patients with DBS.

The Thesis is subdivided into six sections. After the introduction, Section 2 presents the relevant theory: the clinical features and pathophysiology of PD, the instrumentation and clinical considerations related to DBS and its potential mechanisms of action, the instrumentation, interference suppression and source modeling methods of MEG, and, finally, the concept of coherence and previous research on coherence in PD. Then, Section 3 presents the materials and methods employed in the Thesis. Section 4 presents the results, and Section 5 discusses the reliability of the results and their potential implications for future research. Finally, Section 6 summarizes the most important findings.

2 Theory

2.1 Parkinson's disease

Parkinson's disease (PD) is the second most common neurodegenerative disease in Western populations [1]. The incidence of PD increases with age; the prevalence at the age of seventy varies between 0.5 and 2 % in different populations [1, 15]. In Finland, about 12 000 patients are currently treated for idiopathic PD [16]. The disease gradually progresses over 10–25 years starting from minor motor dysfunction and proceeding to severe disability [17]. At present, no tools exist to prevent disease progression, but treatments aim at reducing symptoms and improving the quality of life. This section briefly presents the clinical features and pathophysiology of the disease. A separate section is dedicated to deep brain stimulation, a relatively novel treatment for PD.

2.1.1 Clinical features

PD is most commonly diagnosed between the ages of fifty and seventy, the mean age of onset being 62 [18]. The diagnosis is based on a clinical examination: cardinal symptoms include *tremor*, *bradykinesia*, and *rigidity* [17]. Early PD is often marked by reduced complementary movements on one side of the body; patients with a more advanced disease have a characteristic gait with a stooped posture and small shuffling steps [18].

Low-frequency rest tremor (4–6 Hz) is experienced by 75 % of Parkinson's patients [18]. The tremor typically affects one side more than the other and lessens with voluntary movement but reappears with prolonged strain; the tremor of the hands may resemble a pill-rolling movement [19]. Rest tremor may occur alone or in combination with postural and kinetic tremor. Postural and kinetic tremor appear with voluntary contraction of muscle: postural refers to the static maintenance of position against gravity and kinetic to any dynamic voluntary movement. Deuschl et al. [20] have described different tremor profiles observed in PD:

- **Type I:** classic Parkinsonian tremor: isolated rest tremor or rest tremor with postural/kinetic tremor with the same frequency (> 4 Hz)
- **Type II:** rest tremor and postural/kinetic tremor of different frequencies (difference < 1.5 Hz)
- **Type III:** isolated postural/kinetic tremor (between 4 and 9 Hz)

The postural/kinetic tremor observed in the context of PD is typically mild. In fact, mild kinetic tremor is present in almost all patients. In some cases the postural/kinetic tremor can be disabling; however, it should be noted that severe postural tremor in combination with PD is most often considered a variant of another neurological disorder called *essential tremor*. [20] The patients with Type III isolated

postural/kinetic tremor are classified as having an akinetic-rigid variant of the disease as opposed to a tremor-dominant variant.

Besides the cardinal motor symptoms, patients suffer from reduced facial expressions and blinking, weakened voice, and drooling [17]. Motor symptoms coexist with a variety of nonmotor aspects of the disease. These include lacking sense of smell, sleep disturbances, orthostatic hypotension, mood disorders, and dementia [17].

The term "Parkinson's disease" refers to idiopathic PD, whereas similar symptomatology caused by another neurological disorder is referred to as "atypical Parkinsonism". Diagnoses other than PD that may cause Parkinsonism include multiple-system atrophy, progressive supranuclear palsy, and frontotemporal dementia [17]. A follow-up of approximately five years after the initial diagnosis is therefore considered necessary to reach a reliable diagnosis through precluding alternative causes of Parkinsonism [16].

2.1.2 Pathophysiology

The main pathologic hallmark of PD is the progressive degeneration of a dopaminergic population of neurons in the midbrain structure *substantia nigra pars compacta* (SNc). The SNc directly projects to a set of subcortical nuclei located around the thalamus, collectively referred to as the basal ganglia. These include the *striatum*, the *globus pallidus interna* and *externa* (GPi and GPe, respectively), the *subthalamic nucleus* (STN) and the *substantia nigra pars reticulata* (SNr) (Figure 1). The basal ganglia constitute a complex circuit that regulates voluntary movements through connections to the thalamus and the motor cortex, located in the precentral gyrus of the posterior frontal lobe. As can be observed in PD, the proper functioning of the motor circuit somehow depends on the modulatory actions of SNc-derived dopamine.

The traditional model of PD pathophysiology emphasizes the dual action of dopamine in the basal ganglia. Via two distinct receptor types dopamine increases the responsiveness of one neuronal population while decreasing the responsiveness of another. As a result, dopamine depletion inevitably alters the dynamics between the two populations. The facilitating effect of dopamine mainly targets a neural pathway called the *direct pathway* and the inhibiting effect a parallel pathway called the *indirect pathway* (Figure 2), described, respectively, as the accelerator and the brake of the motor loop. The functioning of the basal ganglia has been thought to be governed by the interplay between the direct and the indirect pathway and PD pathology to result from the imbalance between the two pathways.

Recently, however, a more dynamic model has emerged on PD pathology. Effectively, it has long been known that distinct brain functions and states of arousal are associated with oscillations occurring at specific frequency bands. For example, alpha band activity (8–13 Hz [7]) is known to increase when closing the eyes and when relaxing [22], whereas gamma band (40–50 Hz) cortical activity has been associated with a phenomenon known as perceptual binding involved in object recognition [23].

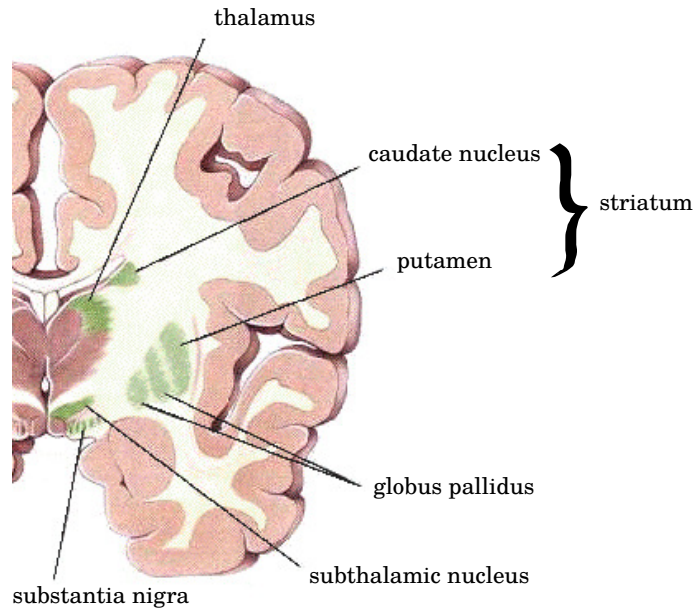


Figure 1: The anatomy of the basal ganglia, the thalamus and the *substantia nigra* (SN). The SN consists of two parts that are anatomically adjacent but functionally different: *pars compacta* (SNc) and *pars reticulata* (SNr). Adapted from [21].

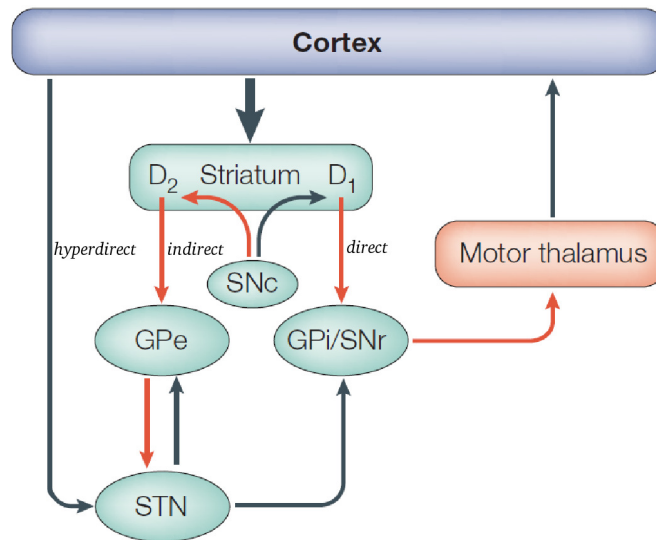


Figure 2: Main synaptic pathways of the basal ganglia motor circuit. Red arrows denote inhibitory connections and blue arrows excitatory connections. D1 and D2 are the different types of dopamine receptors that account for the dual effects of dopamine in the striatum: D1 receptors facilitate signaling in the direct pathway and D2 receptors suppress signaling in the indirect pathway. The hyperdirect pathway has been recently added to the model; most textbooks still refer to only two parallel pathways. Adapted from [7].

Motor function has been associated with cortical oscillations at the beta band (14–30 Hz [7]).

The basal ganglia, like other brain areas, exhibit oscillatory firing patterns; that is, periodic variations in electrical activity that may become synchronized with connected structures, including the cortex and the thalamus. Excessive beta synchrony at the level of the basal ganglia has been associated with PD pathology. Therefore, beta band activity is sometimes referred to as "antikinetic", in particular at the level of the basal ganglia, where beta band is suppressed after treatment with a dopamine precursor, levodopa [8]. Figure 3 illustrates the suppression of beta band and the emergence of oscillations at the high gamma band (> 60 Hz) after the administration of the drug.

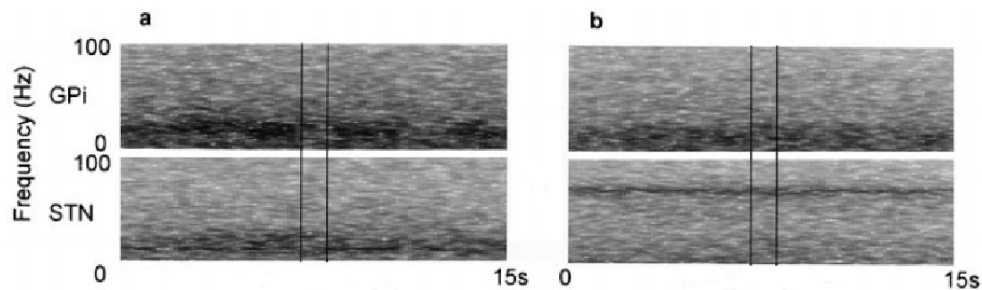


Figure 3: Local field potential recordings in the STN and the GPi by Brown et al. show a change in frequency composition especially in the STN after administering levodopa. Figure **a** presents results off treatment and **b** on treatment. The observed pattern of activity was present both in rest and in voluntary movement. Darker color indicates stronger signal (arbitrary units). Adapted from [8].

Cortical beta activity was associated with motor function by Penfield already in 1954 [10]. Penfield reported that beta activity recorded from the surface of the motor cortex is suppressed during repetitive self-paced movements but reappears with static muscle contraction. Later studies have confirmed that movement execution is accompanied by an event-related beta desynchronization as well as a "post-movement beta rebound" and that these phenomena localize to the sensorimotor areas of the cortex [24].

Since the motor cortex and the basal ganglia are intimately connected, it could be envisioned that abnormal oscillations would spread from the basal ganglia to the cortex altering cortical oscillation patterns. In support of this hypothesis, Heinrichs-Graham et al. [11] have recently shown that both cortical beta desynchronization and beta rebound during movement are diminished in PD patients. They envision that the basal ganglia, due to aberrant oscillations, are unable to efficiently suppress cortical oscillations in anticipation of voluntary movements in PD. The view of PD pathophysiology as a result of aberrant oscillations explicates why both lesions and high-frequency stimulation are able to alleviate PD symptoms: both can disrupt pathological oscillatory patterns [25].

2.2 Deep brain stimulation

Attempts to treat PD with the electrical stimulation of deep brain structures were made in the late 1980s, when Benabid and coworkers discovered that high-frequency stimulation of a thalamic nucleus reduced PD symptoms [3]. Their finding led to the development of the technique known as deep brain stimulation (DBS), which is used to treat advanced PD. The treatment consists of high frequency electrical stimulation either in the STN or the GPi. The STN is nowadays the favored target in PD [16, 26]. Besides PD, medically unmanageable essential tremor and dystonia are being treated with DBS [27].

In Finland, DBS was first employed in the 1990s, and some 1000 patients have been treated since [16]. DBS offers clinical benefits superior to the best available medical therapy for advanced PD [4] as well as PD with early motor complications [28], and the clinical effect may persist up to 10 years of treatment [5, 6]. Yet, the mechanism of action remains unresolved. This section consists of three subsections: the first describes the instrumentation of DBS, and the second reviews the criteria employed in patient selection. The third section discusses the physiological effects of DBS; that is, the yet unresolved puzzle of the mechanisms underlying the therapeutic effects.

2.2.1 Patient selection

Four main criteria should be considered when assessing a surgical candidate for DBS. Firstly, a patient may become a candidate only if their disease no longer responds satisfactorily to medication. Ideal surgical candidates respond well to levodopa but suffer from motor complications that cannot be controlled with medication, and hence cause disability [29]. Unlike other symptoms not responding to levodopa, drug-resistant tremor usually responds well to DBS [16]. Tremor-dominant patients, therefore, constitute a relevant subgroup of surgical candidates.

Secondly, it should be ascertained that the patient suffers from idiopathic PD and not from another form of Parkinsonism. Patients suffering from atypical Parkinsonism may benefit from DBS on the short term, but the progression of their disease may efface the effects quite rapidly [30].

The third criterion entails the fitness of the candidate brain. Preoperative magnetic resonance images (MRIs) are required to assess the quality of the brain tissue in the relevant regions. Considerable brain atrophy or vascular lesions in the basal ganglia serve as exclusion criteria [16]. Considering the stresses of the surgery, the general fitness of the patient also plays a role. For this reason, many centers have set an age limit for patients accepted for surgery. For example, Helsinki University Central Hospital generally excludes patients over 70 years of age from surgical candidacy [16].

Finally, patient cooperation is required both during surgery and after the operation: stimulation adjustment and stimulator maintenance require the patient's active participation. Emotional stability and absence of psychiatric disturbances hence are

prerequisite for successful DBS therapy; similarly, patients with dementia cannot be included for the procedure [30]. To summarize, the preceding criteria can be grouped as follows:

Inclusion criteria

- medication-resistant disability
- good response to levodopa
- follow-up of ≥ 5 years after initial diagnosis
- realistic expectations on treatment efficacy

Exclusion criteria

- age > 70 years
- brain atrophy or vascular lesions especially in the basal ganglia
- poor cooperation
- ongoing psychosis and/or dementia

2.2.2 Instrumentation and surgical procedure

DBS entails the stereotactically guided implantation of a multi-electrode lead into one of the basal ganglia nuclei. A battery-powered pulse generator unit is inserted subcutaneously in the chest to drive the lead. An insulated cable runs subcutaneously from the top of the head to the chest, connecting the lead and the pulse generator. The pulse generator unit can be telecontrolled by bringing a control device over its location in the chest. Figure 4 shows a schematic representation of the DBS hardware.

The main surgical target for deep brain stimulation in PD is the STN [4]. Implantation in the GPi is also employed: it efficiently and immediately decreases dyskinesias but may have poorer long-term effect on motor performance [31]. Another benefit with the DBS of the STN is that it allows for a reduction of medication [32]. For patients with tremor as their only symptom, DBS of the thalamus also represents an option [16]. Surgery is performed bilaterally to alleviate symptoms on both sides [4].

The day before surgery, medication is withdrawn in order to distinguish the effects of the DBS. The leads, measuring a few millimeters in diameter, are placed using minimally invasive stereotactic surgery in which cranial MRIs and computer tomography images are fused to obtain a three-dimensional coordinate system of the patient's brain. The target area is stimulated during surgery to control for the proper positioning of the leads; also, potential side effects are detected thereupon [4].



Figure 4: A schematic representation of a unilaterally implanted DBS electrode and its pulse generator unit. Adapted from [33].

The positioning procedure requires for the patient to stay awake and to be able to cooperate. Clinical experience is needed to choose between thousands of possible combinations of stimulation parameters. The set of stimulation parameters consists of pulse voltage, pulse duration, and frequency, typical values for PD being 2.5–3.5 V, 60–90 μ s, and 130–180 Hz, respectively [34].

After the operation, stimulation parameters are readjusted several times to obtain an optimal response. A remote control can be also used by the patient to adjust the pulse generator. The initial settings are routinely readjusted by the treating neurologist three months and six months after the operation [35]. Meanwhile, medication is gradually reduced [16]. Stimulation readjustment is needed to compensate for the changes that follow the healing of the microlesion produced by the surgery [16]: lesioning *per se* may alleviate the symptoms, and so symptoms may worsen as the lesion heals. Furthermore, disease progression eventually calls for readjusting the stimulation.

Typical DBS leads employ platinum-iridium conductor wire with fluoropolymer insulation and a polyurethane outer jacket [36]. The four platinum-iridium electrode surfaces at the distal tip of the lead can be freely combined to deliver optimal stimulation. The number of surfaces employed directly correlates with current consumption and, thus, inversely with battery life. In practice, a choice is made between a monopolar and a bipolar configuration (Figure 5): the bipolar configuration produces a more localized electric field, theoretically reducing the chance of side effects; however, the monopolar configuration generally produces a more robust clinical effect [16].

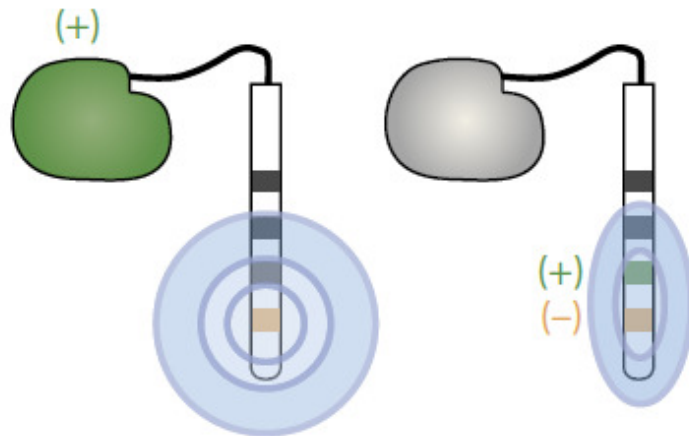


Figure 5: Theoretical illustration of the relationship between the electrode configuration and the geometry of the electrical field: monopolar (left) and bipolar configuration (right) are the most commonly used configurations in DBS. As a courtesy of [16].

Invasive procedures such as stereotactic surgery inevitably carry a risk of intracranial bleeding. The bleeding rate for DBS lead insertion has been reported to vary between 2.0 and 2.5 % [34]. Other hardware related complications include infection, which is the most common hardware related complication in DBS [35], as well as lead dislocation and fracture [34]. Intracranial bleeding may lead to severe disability, even death, while the other complications inevitably lead to device removal. The severity of these risks is the main reason for which DBS cannot be prescribed as routinely as medication.

2.2.3 Effect on physiology

DBS, when correctly applied, is able to relieve all cardinal symptoms of PD (bradykinesia, tremor, and rigidity) [4]. In addition, DBS efficiently tackles dyskinesias and motor fluctuations [32], which often accompany prolonged treatment with levodopa, the gold standard in pharmacotherapy for PD. As a general rule, DBS mainly alleviates symptoms that respond to levodopa [4]. However, levodopa-resistant tremor is known to refute the rule [30].

Despite the prominent clinical effect, the mechanisms through which DBS modifies brain activity and thereby alleviates Parkinsonian symptoms is poorly understood. Modeling studies suggest that clinically effective DBS parameters result in stimulating a large volume of neural tissue that extends beyond the target nucleus (usually the STN) into the adjacent *capsula interna* fibers, which connect the cortex with the thalamus and the brainstem [37]. The electrophysiological properties of passing axonal fibers support their role as potential stimulation targets [34].

It has been debated whether DBS excites or inhibits neurons and whether it affects synapses or passing axonal fibers (see [34] for discussion). Synaptic inhibition would

explain the similarity between the effects of lesioning and high-frequency stimulation [4]. On the other hand, primate studies have shown an activation of the excitatory pathway between the STN and the GPi [38]. In contrast, stimulation-related secondary effects such as speech difficulties (dysarthria), abnormal sensation (paresthesia), double vision (diplopia), and muscle spasm (dystonia) are compatible with the putative stimulation of the passing fibers [16].

It is likely that DBS, as a function of distance from the stimulation site, produces both neuronal excitation and inhibition. The temporal characteristics of the applied stimulation appear crucial: both low- and high-frequency stimulation in the primate model of PD produced multiphasic neuronal responses with alternating periods of inhibition and excitation but only the high-frequency stimulation was able to alleviate the clinical signs of PD [34].

The prevailing idea is that high-frequency stimulation somehow overrides pathological spike patterns in the basal ganglia. Beta activity, in particular, is believed to be suppressed in the basal ganglia during DBS. Findings like those by Kühn et al. [9] support this idea: they demonstrated that beta activity was suppressed in the STN several seconds after therapeutic high-frequency stimulation at the same time as patients continued to experience improvement in hand movements.

For the clinical effect to appear, the changes achieved in the basal ganglia probably somehow affect cortical signaling. In this vein, the leading candidate mechanism for DBS is the disruption of pathological beta activity within the cortex [11]. Supporting this view, Kühn et al. [9] showed that immediately after DBS cessation the coherence between the cortex and the STN was reduced at the beta band and that this reduction correlated with motor performance.

Airaksinen et al. [39] reported that signal strength between 10 and 20 Hz could either increase or decrease depending on the patient when DBS was turned off. Nevertheless, they witnessed in the on-treatment condition a correlation between the degree of beta activity and the rigidity score. To summarize, an understanding of the physiological effects of DBS requires further studies on all levels of the motor loop. One of the aims of this Thesis is to look into the cortical effects of DBS in the context of a static motor task.

2.3 Magnetoencephalography (MEG)

Magnetoencephalography (MEG) measures changes in magnetic field patterns outside the head. Once all contribution from external magnetic sources has been eliminated, the measured fields reflect electrical signaling in the brain, especially the cortex. To detect the extremely weak magnetic fields, MEG employs superconductive coils that can detect current elements down to the order of 10 nAm [40]. In addition to its sensitivity, MEG has excellent temporal resolution, which makes it a useful tool for the study of cortical oscillatory patterns, such as those implicated in motor impairment in PD, as described in Section 2.1.2. This section discusses MEG instrumentation, data preprocessing and source modeling methods, and the neural correlates of MEG.

2.3.1 Neural correlates of MEG

Nerve cells or neurons are the smallest information processing units in the brain. Neurons can be functionally and structurally subdivided into three distinct parts; they consist of dendrites that receive information from other neurons, a cell body or soma that integrates information, and an axon that conveys the output of the neuron to other nerve cells. Information transfer in neuronal populations combines chemical and electrical signal transmission.

Chemical transmission takes place at synapses between cells: the binding of a chemical transmitter to a dendritic ending causes ion channels in the cell membrane to open producing a shift in the membrane potential called a *postsynaptic potential*. The change in the membrane potential gives rise to a current flow along the dendrite towards the soma. The summation of postsynaptic currents at the soma may trigger a dramatic, self-propagating rise in membrane potential, an *action potential*, that spreads rapidly along the axon.

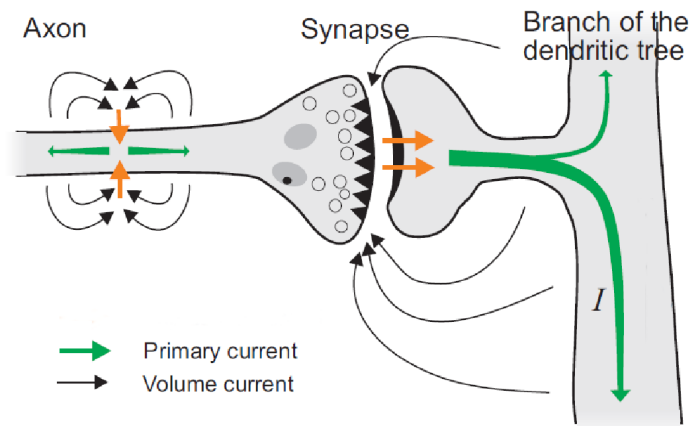


Figure 6: The green arrows on the left represent axonal currents and those on the right postsynaptic currents, both of which are classified as *primary currents*. Primary currents, especially those in the dendritic tree, are the primary source of MEG signal. Volume currents (black arrows) are ohmic currents that compensate for the intracellular currents by transferring charge through the extracellular volume. Adapted from [41].

The intracellular currents that accompany the axon potential spread simultaneously in two opposing directions almost symmetrically (Figure 6) forming a quadrupole current constellation the magnetic field of which decays rapidly (as $1/r^3$). Synaptic currents are bipolar by nature and decay very quickly. Therefore, axon potentials and synaptic currents contribute relatively little to the magnetic field detected with MEG. Postsynaptic potentials, by contrast, travel unidirectionally in many parallel dendrites and decay more slowly than axon potentials (as $1/r^2$) allowing for spatial and temporal summation to occur. Postsynaptic potentials in synchronously

activated neurons are thereby likely to make the greatest contribution to MEG signal. [41]

Murakami and Okada [42] have studied the contributions of different cortical cell types to the MEG signal. They conclude that cortical pyramidal cells are likely to contribute the most to MEG signal. Pyramidal cells are an abundant cell type of the neocortex; one well-documented function is their role as upper motor neurons of the corticospinal tract that controls voluntary movements. Pyramidal cells have a large dendritic tree consisting of apical dendritic branches and basal dendrites.

Cortical activity at a small distinct area of neural tissue is often described as a current dipole. Measurable cortical activity is generally on the order of 10 nAm (10^{-8} Am) [40]. Murakami and Okada estimate that single pyramidal neurons produce an intracellular current dipole on the order of 10^{-12} Am, that is, 10^4 times weaker than what is detectable. Hence, they estimate that 10 000–50 000 pyramidal cells need to activate synchronously for the resulting magnetic field to be detectable by MEG [42].

2.3.2 Instrumentation

The weak neuromagnetic fields of the brain require an especially sensitive detector. To reach sufficient sensitivity, modern MEG devices employ superconductive quantum interferences devices (SQUID) immersed in liquid helium ($T = 4.2$ K). A SQUID (Figure 7) consists of a superconductive loop interrupted by thin layers of electric insulator. The weak links that are thus created are called *Josephson junctions* [40]. Paired electrons may tunnel through the links giving rise to a quantum interference phenomenon that produces a measurable physical quantity; namely, a dynamic resistance across the coil [43].

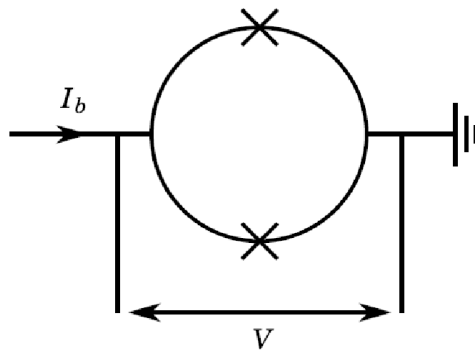


Figure 7: A schematic representation of a SQUID. The voltage V is kept constant by applying a negative feedback current I_b to the loop. Adapted from [44].

The dynamic resistance and thereby the voltage across the SQUID depend non-linearly but periodically on the applied flux (Figure 8). Due to the periodicity of the flux–voltage relationship, adding exact multiples of the flux quantum to the

loop does not alter the measured voltage. Thus, to calculate absolute flux values, one would need to keep track of the periodic cycles — instead, the changes in flux are detected by keeping the SQUID at a constant operating point (dashed line in Figure 8) by applying a negative feedback current to the loop [43]. That is to say, the SQUID output is kept at zero, while the negative feedback current fluctuates according to the measured flux.

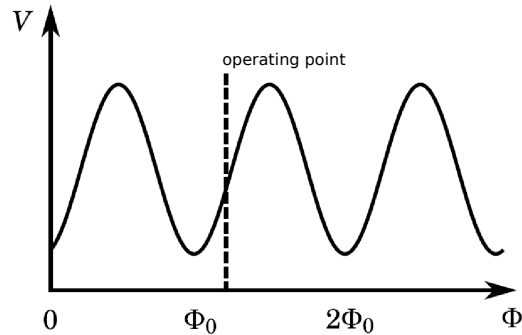


Figure 8: The periodic flux–voltage relationship of a SQUID: adding a multiple of the flux quantum (Φ_0) does not change SQUID voltage. The dashed line indicates a suitable operating point in which a change in the flux induces a maximal change in SQUID voltage. Adapted from [44].

To reach optimal sensitivity, SQUIDS are made small, typically less than 1 mm in outer diameter, leading to a very limited coverage of the magnetic field of interest [43]. To improve the coupling of the SQUIDS to the magnetic field, they are connected to *flux transformer* coils that collect magnetic flux from a much larger area. Flux transformers consist of a large pick-up coil ($d \approx 2\text{--}3$ cm [41]) and a smaller multiturn signal coil connected in series.

Different pick-up coil geometries can be used to measure different components of the magnetic field (Figure 9). The simplest configuration, a magnetometer, consists of a single loop that measures the magnetic field component perpendicular to the plane of the coil, that is, B_z . Gradiometers, by contrast, have two loops wound in opposite directions. The loops of an *axial gradiometer* are aligned along the same axis forcing fields that are constant along the axis to cancel each other. If the two loops are in a plane, the sensor is a *planar gradiometer*. Axial gradiometers are sensitive to fields that change along their axis, $\delta B_z/\delta z$, while planar gradiometers detect changes across the plane of the loops, $\delta B_z/\delta x$.

Due to the pick-up coil geometry, gradiometers are relatively insensitive to faraway interference sources that manifest themselves to the sensors as nearly homogeneous. Magnetometers, on the other hand, are sensitive both to nearby brain sources and distant interference sources. Magnetometers also have better sensitivity to sources located deep in the brain. The sensitivity of a single sensor to a particular current distribution can be expressed as a *lead field* (Figure 10). The lead field can be used to assess the signal strength at the sensor produced by a single dipolar source by projecting the dipole onto the lead field. As Figure 10 demonstrates, signals

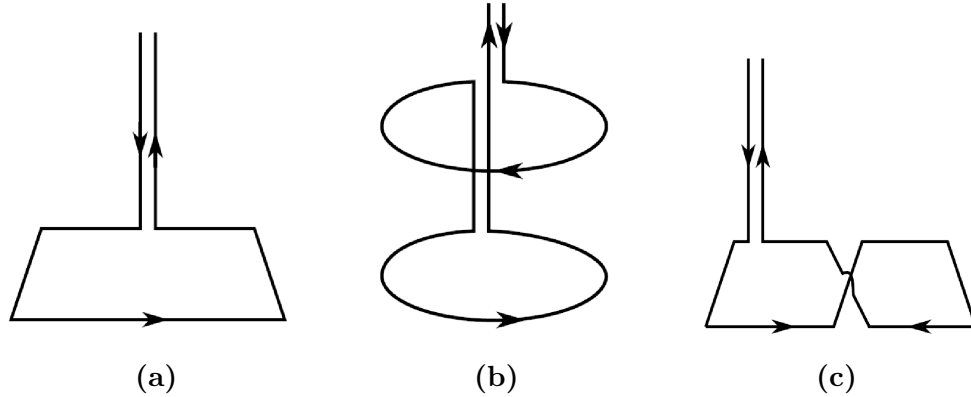


Figure 9: Pick-up coil geometries: (a) magnetometer, (b) axial gradiometer, (c) planar gradiometer. Adapted from [44].

from both magnetometers and axial gradiometers peak for sources around the rim of the pick-up coil; planar gradiometers, by contrast, peak when directly on top of the source [43]. The lead fields of two orthogonal planar gradiometers and a magnetometer at the same location and plane are all orthogonal, meaning they provide independent information about the measured field.

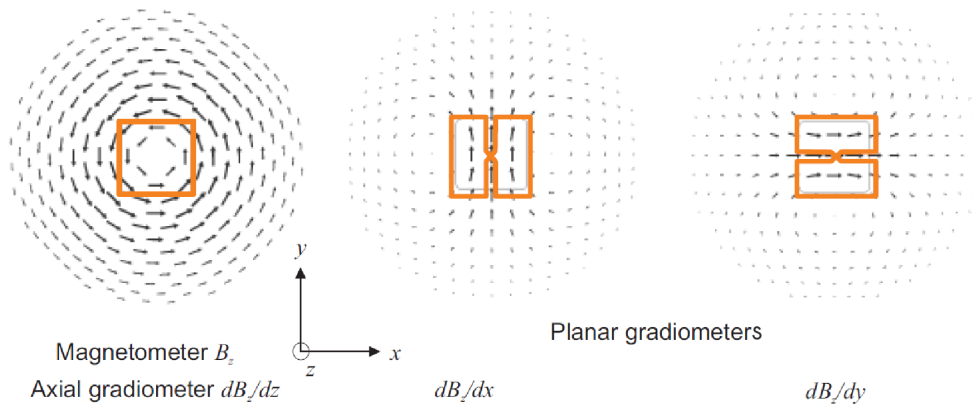


Figure 10: Lead fields corresponding to different pick-up coil geometries. Adapted from [41].

2.3.3 Interference suppression

The extracranial magnetic fields produced by neural sources are extremely weak: compared to the Earth's magnetic field (50–90 μT), the brain physiological evoked responses, typically on the order of magnitude of 100 fT [41], are about 10^8 times weaker (Figure 11). Other interference sources that exceed brain-originating magnetic fields by several orders of magnitude (Figure 11) include ambient sources such

as powerlines (at 50 Hz and its harmonics), large moving magnetic objects such as passing cars and elevators, and biological sources such as the heart, the skeletal muscles, and the eyes. Dental fillings and magnetic implants also cause interference whenever the subject is moving. In this Thesis, artefacts caused by DBS required special attention.

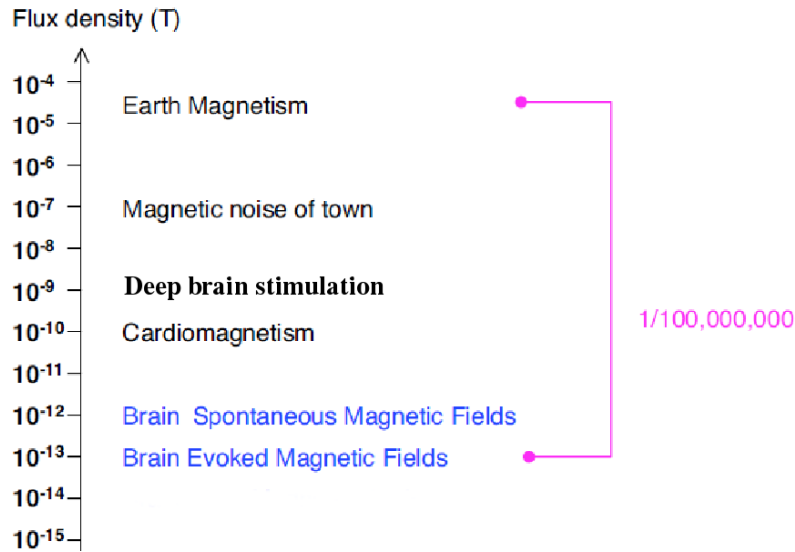


Figure 11: Amplitudes of neurophysiological and ambient magnetic fields. Adapted from [45].

Signal interference can be suppressed by passive and active magnetic shielding and by computational noise-cancellation. Here, special emphasis is placed on a particular computational noise-cancellation method, the *signal space separation* method (SSS) [46], and its extension, the *temporal signal space separation* method (tSSS) [14], as they effectively cancel interference caused by DBS.

Passive shielding

Passive magnetic shielding is achieved by placing the MEG device inside a magnetically shielded room. The walls of the room contain alternating layers of high permeability mu-metal and aluminium; the former provides the external magnetic fields a low reluctance path along the walls, and the latter favors the formation of eddy currents that counteract the penetrating fields [41].

Active shielding

Passive shielding can be enhanced by active shielding systems: the interference field is measured and a compensating field is generated to cancel the interference outside the room. Because it does not take into account the spatial inhomogeneities of the

external fields, active shielding is only effective against relatively distant sources (\geq tens of meters). [41] The shielded room in the BioMag laboratory, used for the measurements in this Thesis, relies on traditional three-layer passive shielding with no active shielding systems.

Computational noise-cancellation

Computational methods can be used to discern interference in the collected data. The SSS method [46] separates signals that originate outside the sensor helmet from signals originating inside the helmet based on the physical properties of magnetic fields defined by the Maxwell's equations and the measurement geometry. Based on quasistatic Maxwell's equations [40], a fundamental linear basis can be created that spans all measurable signals of magnetic origin. As a result, any magnetic field (\mathbf{B}) located in a source-free volume (eg. the space that contains the MEG sensors) can be expressed in any point \mathbf{r} in spherical coordinates as a general series expansion [44]:

$$\mathbf{B}(\mathbf{r}) = \sum_{l=0}^{\infty} \sum_{m=-l}^l \alpha_{lm} \frac{\boldsymbol{\nu}_{lm}}{r^{l+2}} + \sum_{l=1}^{\infty} \sum_{m=-l}^l \beta_{lm} r^{l-1} \boldsymbol{\omega}_{lm}, \quad (1)$$

in which r is the length of \mathbf{r} and denotes the distance from the expansion origin (Figure 12). Symbols $\boldsymbol{\nu}$ and $\boldsymbol{\omega}$ denote modified vector harmonic functions in the spherical coordinate system [46]. The shape of the functions changes with indices l and m . Coefficients α and β are defined when fitting the series expansion to match the magnetic field.

The two series expansions in Equation 1 have different convergence volumes [46]; the first term increases with decreasing r , while the second term increases with increasing r . This implies brain sources located inside the helmet are contained in the first expansion, the *inside expansion*, while external sources are contained in the second expansion, the *outside expansion*. Accordingly, interference suppression is achieved by reconstructing the sensor data by using only the inside expansion. A truncated version of the expansion is used to match the noise level of the sensors used in the MEG device [43].

Two main factors can produce inaccuracies in the reconstruction process: (1) inaccuracies in sensor calibration and (2) the finite truncation of the series expansion [14]. The error caused by the truncation of the series expansion is usually insignificant provided there are no sources in the immediate vicinity of the sensors [46]. Namely, interference sources located in the volume between the inside and the outside volume ($r_{min} < r < r_{max}$), which contains the sensors, cannot be perfectly reconstructed with the two expansions and result in *signal leakage* between the two expansions. However, signal leakage also occurs with any strong interference source relatively close to the sensor space.

When performing MEG on subjects who have DBS, severe signal leakage inevitably

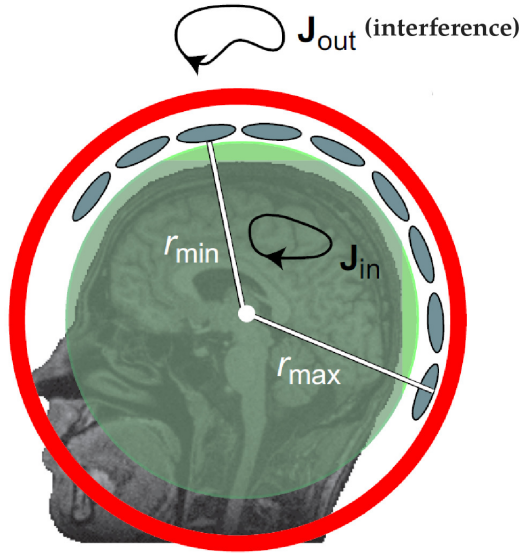


Figure 12: The signal space separation method: the white dot denotes the expansion origin and r_{min} and r_{max} define the inside volume ($r < r_{min}$) and the outside volume ($r > r_{max}$), respectively. \mathbf{J}_{in} and \mathbf{J}_{out} represent current densities in the two volumes. Adapted from [45].

occurs due to the magnetic hardware and the strong electrical currents used in the stimulation. Therefore, in the case of DBS, signal space separation cannot suppress all relevant artefacts. In fact, an extension of the method is required called *temporal signal space separation* or tSSS [14], which, faithful to its name, utilizes temporal information to detect interference signals that SSS alone cannot recognize.

The tSSS method consists of a statistical analysis performed in the time domain that detects signal components having identical temporal behavior in the outside and the inside volume [14]. Since the presence of temporally correlated signal components in the outside and the inside expansion indicates either signal leakage or the presence of sources that, unlike brain signals, behave identically in both volumes, temporally identical components can be safely removed from the data without interfering with signals of interest. Once the temporal analysis has been performed, tSSS projects the SSS-reconstructed data into the orthogonal complement of the previously determined temporally correlated signal components.

Unlike passive and active shielding methods, which act by preventing certain magnetic fields from reaching the sensors, computational methods such as SSS and tSSS are employed after the measurement. Hence, no signal is discarded during data collection, except for signals that exceed the dynamic range of the amplifiers used in the system. Once interfering signals have been suppressed to a satisfactory level, it can be assumed that most of the remaining data reflects neuronal activity. Methods to locate the source of the activity in the brain are discussed in the next subsection.

2.3.4 Source modeling

The forward problem of describing the magnetic field pattern for a known current distribution yields a unique solution. The Maxwell's equations dictate the solution provided that the geometry and the conductivity profile of the source volume are known. The conductivity profile of the human head can be approximated by making assumptions on its shape and tissue properties. A sphere fitted to the inner curvature of the skull is a relatively good approximation of brain geometry; a boundary element method (BEM) that fits a triangular mesh onto the brain volume [47] yields a more accurate model and is used in this Thesis. As for the tissue conductivities, a homogeneous conductor model has been shown to be a good approximation [40].

Unfortunately, the *inverse problem* of estimating current sources from a known magnetic field pattern cannot be uniquely solved. In fact, as von Helmholtz concluded in 1853 [48], a current distribution inside a conductor cannot be derived from knowledge of the electromagnetic field outside. An infinite number of current distributions could explain the field pattern observed outside the head. Due to the non-uniqueness of possible solutions, the search for solutions must be limited by a set of boundary conditions that reflect our understanding of neuronal sources.

Three source modeling methods are presented here: (a) dipole fitting, (b) minimum norm estimation, and (c) beamforming. Source estimation in this Thesis employs the last, a *linearly constrained minimum variance* (LCMV) beamformer.

a. Dipole fitting

Source modeling utilizes the information of the forward solution and the predefined boundary conditions to locate neuronal sources in the brain. The traditional method is to fit a single dipolar source, an equivalent current dipole, to the data by a nonlinear least-squares search [40]. If several simultaneous sources are presumed to be present, the ensemble of sensors can be divided into subpopulations each of which is assumed to reflect the behavior of a single source. Hence, dipole fitting is sensitive to multiple sources only if they are explicitly sought for and affect roughly non-overlapping sensor populations.

b. Minimum norm estimation

Besides dipole fitting that assumes a focal source model, there are methods available that produce a distributed estimation of the source, or a "spatial map of the activity" [41]. In these methods a computational voxel grid is created that spans the brain volume. One way then to model the source distribution is a minimum norm estimate which entails the fitting of a dipole to every voxel in a way that minimizes a cost function containing two terms: the deviation of the estimate from the measurements and the total sum of dipole strengths [41]. The source space can either cover the entire brain volume or be constrained to the cortex [43].

c. Beamforming

Another way to achieve a distributed source estimate with no *a priori* assumptions about the number of sources or their spatial distribution is to use a spatial filtering technique called *beamforming*. Beamformers were traditionally used in radars to catch signals of interest by blocking transmission from all but one predefined location. Van Veen et al. [49] have described the use of beamformers in localizing sources of brain electrical activity. The discussion here follows their description of an LCMV beamformer.

The central idea of beamforming is to reconstruct the source signal as a weighted sum of the sensor signals. The reconstructed source signal is called the *virtual electrode* [50]; it is a dipolar source \mathbf{q} located in a voxel of interest that can be expressed in the time domain as follows:

$$\mathbf{q} = \mathbf{w}^T \mathbf{X} = w_1 \mathbf{x}_1 + w_2 \mathbf{x}_2 + \dots + w_{N_s} \mathbf{x}_{N_s}, \quad (2)$$

in which $w_1 \dots w_{N_s}$ are weights corresponding to sensors $1 \dots N_s$. The data matrix \mathbf{X} consists of vectors $\mathbf{x}_1 \dots \mathbf{x}_{N_s}$ that contain the sensor signals at sample points $1 \dots N$. For the MEG device used in this Thesis, $N_s = 306$.

Note that the Equation 2 represents a *scalar beamformer* in which only one source orientation is considered. Although this Thesis employs a *vector beamformer*, which considers two orthogonal orientations for each voxel, the scalar beamformer is chosen here for simplicity to demonstrate the general principles of the method. We assume here that the direction of the dipolar source is known and limit the treatment to the source strength.

The solution of the forward problem for a given source, as described earlier, only requires information about the geometry and the conductor properties of the conductor volume. The forward solution is employed in beamforming to model the projection of any given source to the sensors. A voxel-specific vector \mathbf{h} is created to contain this projection, that is, the voxel-specific forward solution. The relationship between a source \mathbf{y} and the sensor signals becomes

$$\mathbf{X} = \mathbf{h} \mathbf{y}, \quad (3)$$

in which \mathbf{X} is again the data matrix. Figure 13 illustrates the projection of a source \mathbf{y} to a subset of sensors (sensor signals $\mathbf{x}_1 \dots \mathbf{x}_5$).

The inverse problem is tackled in beamforming by defining a set of sensor weights for each voxel, so that by multiplying the sensor signals by the corresponding weights, we get the source activity in a given voxel. The set of weights ($\mathbf{w} = [w_1 \dots w_{N_s}]^T$) can be thought of as a spatial filter that passes as much of the signal that originates in the voxel of interest as possible while blocking as much of other sources as possible.

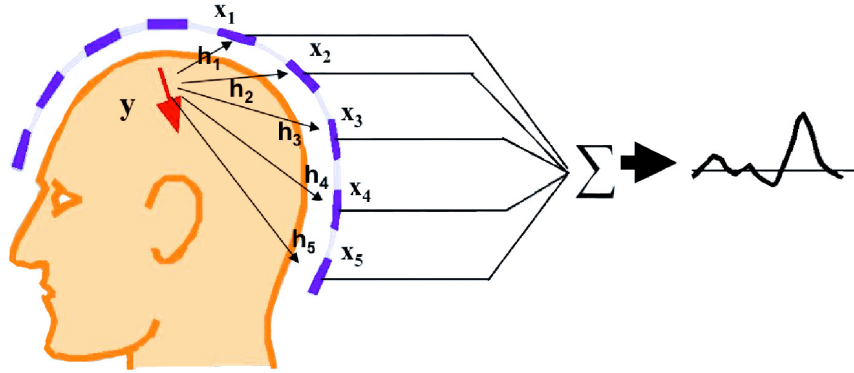


Figure 13: The forward solution of a known voxel \mathbf{h} is used to model the projection of a source \mathbf{y} to the sensors 1...5. Weights $w_1...w_5$ are assigned so that we get an estimate of the source by multiplying the sensor signals $\mathbf{x}_1...x_5$ by the weights. Adapted from [51].

LCMV beamformers employ two optimization criteria to estimate the weights:

1. The weights must pass signals that correspond to the forward solution of a given voxel.
2. The weights must minimize in each voxel the contribution of sources located in other voxels.

The first is achieved by requiring

$$\mathbf{w}^T \mathbf{h} = 1. \quad (4)$$

The second criterion minimizes the contribution of other sources by minimizing the source variance. By assuming zero mean, the signal variance, $Var(\mathbf{q})$, can be calculated by the dot product: $\mathbf{q}\mathbf{q}^T$. By applying Equation 2, the variance can be expressed as follows:

$$Var(\mathbf{q}) = \mathbf{w}^T \mathbf{X}\mathbf{X}^T \mathbf{w}. \quad (5)$$

The matrix product $\mathbf{X}\mathbf{X}^T$ represents the data covariance matrix, \mathbf{A} . Now, the second criterion is met by the following minimization criterion:

$$\min \mathbf{w}^T \mathbf{A}\mathbf{w}. \quad (6)$$

The preceding equation describes the data in the time domain. In this Thesis we employ frequency domain analysis, which entails the transformation of the variables into the frequency domain by using the discrete Fourier transform, defined for a digital signal $x(n)$ that consists of N samples as

$$X(f) = \sum_{n=0}^N x(n)e^{i2\pi fn}, \quad (7)$$

where f is the frequency, i is the imaginary unit and n is the sample number. The transformation is performed in segments using the Welch's method in which a window function is applied that suppresses signals at both ends of the segment. To avoid information loss the segments are overlapping. The Fourier transform produces an estimate of signal power, or spectral density, at each discrete frequency range, or bin. Frequency resolution of the transform is defined by the bin width.

Beamformer analysis is performed in the frequency domain for one bin at a time (width ≈ 1 Hz). To apply Equation 6 in the frequency domain, we need to replace the data covariance matrix \mathbf{A} by the frequency domain equivalent, the cross-spectral density matrix, \mathbf{G} . Cross-spectral density at frequency f is defined for two Fourier transformed signals $X_a(f)$ and $X_b(f)$ as

$$G_{ab}(f) = \langle X_a(f)X_b^*(f) \rangle, \quad (8)$$

where $\langle \rangle$ denotes the expected value, or the average across time intervals, and $*$ indicates complex conjugation. Cross-spectral density G_{ab} can be regarded as the frequency domain equivalent for covariance for signals a and b at frequency f . Using Equations 4 and 6 transformed into the frequency domain, beamforming optimizes the sensor weights to generate in each voxel a virtual electrode, \mathbf{p} , which contains the reconstructed signal power at each time interval at the designated bin. The beamformer-estimated virtual electrodes are referred to as source-space signals in this Thesis.

The resolution of the beamformer method mainly depends on three factors: the density of the voxel grid, the signal-to-noise ratio (SNR) of the data, and the distance from the presumed source to the sensors [49]. Superficial sources are hence estimated with greater precision than deep sources. The lower the SNR, the larger is the spread of the source estimate [43]. Hence, the size of the spread does not describe the true dimensions of the brain activity; rather, it reflects the SNR of the data.

2.4 Coherence

Synchronized neural oscillations are widely considered necessary for neural communication and are thought to reflect functional connectivity between different areas of the brain (see [7] for a review). As described in Section 2.1.2, alterations in the synchronous signalling of the basal ganglia and the motor cortex have been associated with PD pathophysiology. Signaling between the motor cortex and the musculature is similarly critical to motor control. Muscle activity is relatively easy to measure by means of electromyography (EMG) and sensitive accelerometers that track movement. Therefore, a practical way to study motor function is to correlate

cortical signaling, measured with MEG, with peripheral signals, such as EMG. Linear correlation between signals can be assessed with *coherence*. This section presents two distinct coherence measures, corticomuscular and corticokinematic coherence, as potential measures of motor function in PD.

2.4.1 Magnitude squared coherence

Coherence is a frequency domain measure of correlation between two signals. Let $X_a(f)$ and $X_b(f)$ be Fourier transformed signals a and b with a cross-spectral density $G_{ab}(f)$ as defined in Equation 8. Magnitude squared coherence at frequency f is then

$$C_{ab}^2(f) = \frac{|G_{ab}(f)|^2}{G_{aa}(f)G_{bb}(f)}, \quad (9)$$

where $G_{aa}(f)$ and $G_{bb}(f)$ denote autospectral density, which can be considered the frequency domain equivalent of variance. Note that all quantities are averages over a number of time intervals (see Equation 8). Coherence values range from zero to one. A value of one suggests that the two signals behave identically; i.e., their relative amplitudes and phase difference remain constant. By contrast, signals with opposite phase will produce a coherence score of zero. The coherence scores reported in this Thesis represent magnitude squared coherence.

2.4.2 Corticomuscular coherence

Neurons in the primary motor cortex send axons to the spinal cord where they connect to alpha motor neurons that innervate skeletal muscles on the contralateral side of the body. The neurons give rise to the corticospinal pathway that is responsible for the generation of voluntary movements. One way to study the functioning of the pathway is to assess coherence between the two ends, the motor cortex and the skeletal muscle. When coherence is calculated between MEG and EMG, the coherence measure is entitled MEG-EMG coherence or, alternatively, corticomuscular coherence (CMC). In this Thesis we measure CMC between EMG and source-space estimates of MEG sensor signals obtained by beamforming.

The term MEG-EMG coherence was established in 1995 by Conway et al. [12] who demonstrated using single-channel MEG that rhythmic cortical activity associated with sustained contraction was coherent with the electrical activity of the contracting muscle. Significant coherence was observed in all subjects, but the peak frequency and amplitude showed large individual variation: peak coherence occurred within the range 14.5–28 Hz [12]. Figure 14 presents the experimental setting used by Conway et al. and their main results. Salenius et al. [52] confirmed the finding in 1997 with whole-head MEG. They performed dipole fitting to demonstrate that the cortical sources were localized at the motor cortex. In addition, having recorded EMG in

upper and lower limb muscles, they were able to show a clear spatial distinction between source areas related to hand and foot movements.

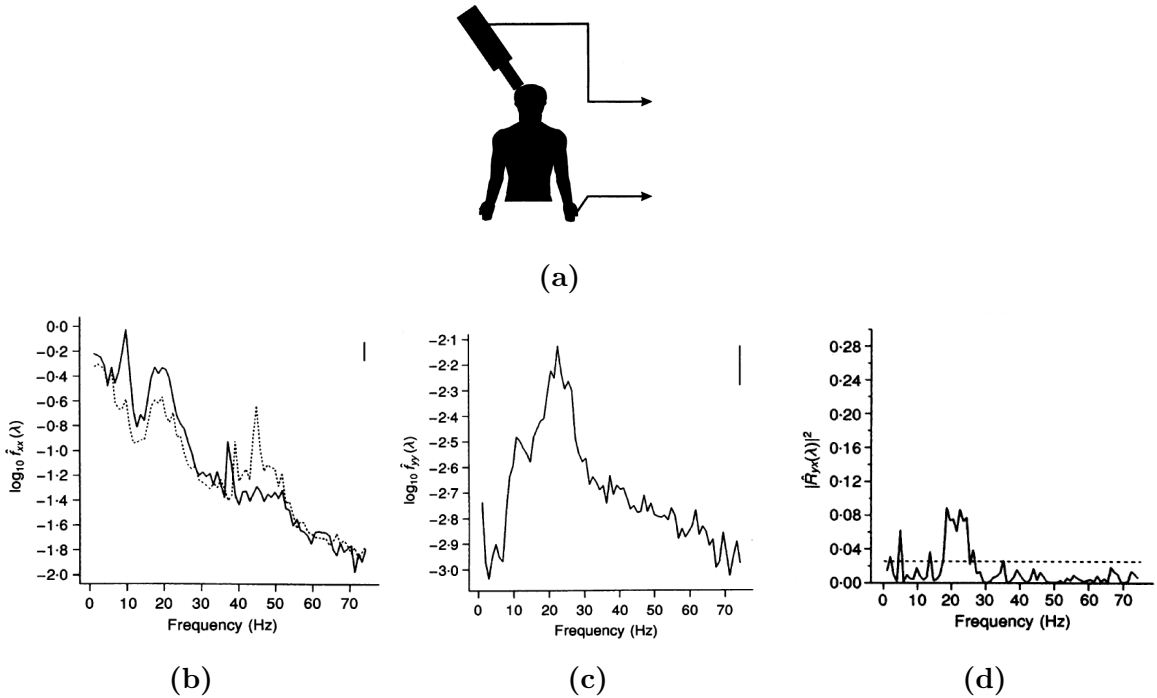


Figure 14: The demonstration of MEG-EMG coherence by Conway et al.: (a) the experimental setting showing the MEG sensor positioned over the contralateral motor cortex of the task-performing hand, (b) estimated MEG autospectrum with the subject relaxing (continuous line) and with the subject maintaining a contraction of the contralateral hand (dotted line), (c) estimated EMG autospectrum with maintained muscle contraction of the hand muscles, and (d) MEG-EMG coherence during muscle contraction. The vertical lines represent 95 % confidence intervals. Note the use of logarithmic scale. Adapted from [12].

It should be noted that both Conway et al. [12] and Salenius et al. [52] observed coherence also at frequencies outside the beta band. The EMG spectra showed peaks roughly at 10 Hz (alpha), 20 Hz (beta), and 40–50 Hz (gamma band), and significant coherence was present at all three bands. However, alpha and gamma band coherence peaks were occasional findings, only present in a minority of subjects. Interestingly, alpha band coherence has been associated with PD rest tremor of the same frequency, while gamma band coherence has been linked with very strong muscle contractions [53]. Here, we limit our scope to beta band coherence, not least because of the accumulated reports on aberrant beta synchrony in PD at multiple levels of the motor loop.

2.4.3 Corticomuscular coherence in Parkinson’s disease

Defective MEG-EMG coherence at the beta band has been demonstrated in PD. Salenius et al. [13] studied eight patients withdrawn from antiparkinsonian medication and showed that only two out of eight had significant coherence between 15

and 30 Hz. However, after treatment with levodopa, six out of eight displayed significant coherence. In some patients, strong peaks between 3 and 12 Hz disappeared with treatment, whereas in others a weaker peak appeared below 10 Hz after the administration of the drug.

Caviness et al. [54] have studied coherence associated with small-amplitude postural tremor often present in PD. Patients with or without visible postural tremor were compared with healthy controls with or without physiological postural tremor during wrist extension. Hand tremor was recorded using an accelerometer attached to the dorsum of the hand. Both groups with postural tremor showed a peak in the accelerometer spectra at 6–7 Hz, presumably associated with the visible tremor. The study showed increased coherence between 12 and 18 Hz in the PD group with postural tremor when compared to the other groups. The finding suggests a cortical involvement in PD postural tremor that is different from healthy individuals.

The first study to measure CMC in PD patients using DBS was recently published by Park et al. [55]. The study showed an increase in CMC when DBS was applied in three patients during moderate strength isometric contraction. The patients in the study all suffered from Parkinsonian rest tremor that was alleviated by DBS. Airaksinen et al. [56], who studied a cohort of nineteen patients, obtained less consistent results on the effects of DBS on CMC: they saw both increases and decreases in CMC when DBS was switched off.

The results by Airaksinen et al. show large individual variation: only eleven out of nineteen patients had significant coherence between 13 and 25 Hz both with DBS on and off, another two patients had coherence only with DBS on and an interesting group of two only with DBS off. The authors note that all patients who showed significant coherence in both conditions had an akinetic-rigid variant of PD as opposed to a tremor-dominant variant. Although their results seem more ambiguous than those by Park et al., they, too, promote the idea of CMC reflecting motor function in PD. Airaksinen et al. [56] show that the CMC peak amplitude correlates negatively with tremor scores when DBS is switched off, indicating that patients with less tremor have stronger CMC, as suggested by Park et al.

2.4.4 Corticokinematic coherence

Bourguignon et al. [57] introduced corticokinematic coherence (CKC) as a novel tool for the functional mapping of the motor cortex in 2011. CKC is calculated between a cortical signal (MEG) and a three-axis accelerometer signal recording the kinematics of a voluntary movement. Bourguignon et al. showed that when subjects were performing self-paced repetitive finger movements, a coherence peak appeared at the movement frequency and its first harmonic. A related study localized the source of the coherence in the sensorimotor cortex, either close to the "hand knob" of the primary motor cortex or slightly posterior to it at the primary sensory cortex [58].

Sensitive accelerometers are able to detect the slight postural tremor observed in PD as well as in healthy individuals. Therefore, they represent an ideal tool for the study

of differences in motor function between patients and healthy controls. In addition, if CMC somehow contributes to movement kinematics, the comparison between CMC and CKC could potentially reveal a common cortical component. In this Thesis, we measure CMC and CKC during sustained contraction in patients with DBS on and DBS off and compare the results with those obtained in healthy controls. To our knowledge, no previous studies have looked at CKC during sustained muscle contraction in PD and in healthy subjects.

3 Materials and methods

The methods used in this Thesis were aimed at comparing CMC and CKC in PD patients and in healthy controls. MEG was used to measure cortical activity, and EMG and accelerometers were used to record muscle activity and hand postural tremor. MRIs were coregistered with MEG landmarks to enable source localization. In addition, the severity of the patients' motor symptoms was assessed using a clinical rating scale. Because of DBS, special emphasis was placed on interference suppression. To verify the effectiveness of interference suppression by tSSS, we analyzed sets of phantom data to visualize remaining stimulation-related artefacts and compared these artefacts with patient data.

The data analysis first employed spectrum analysis to compare the accelerometer and EMG spectra and to detect spectral peaks related to postural tremor and to coherence at the beta band. Then, sensor-level coherence spectra were calculated to single out coherence maxima. Finally, beamforming was used to estimate source-space signals and coherence at the 6-Hz band surrounding the frequency of maximum sensor-level coherence. The statistical significance of the source-space coherence maxima was assessed using surrogate statistics.

3.1 Subjects

Ten healthy subjects (6 male and 4 female) aged between 22 and 58 years (mean age = 30 years) volunteered as controls for the study. Six patients were initially selected (5 male and 1 female) but three of them had to be rejected due to excessive tremor observed in the data. The remaining three patients (2 male and 1 female), who qualified for the study, had an akinetic-rigid variant of PD and were aged between 47 and 61 years (mean age = 52 years).

All patients had bilateral deep brain stimulators implanted in the STN (Medtronic Activa PC, Medtronic Inc., Minneapolis, MN). Stimulation parameters are listed in Table 1. In addition to DBS, the patients were on their usual anti-Parkinsonian medication. The study was approved by the Ethics Committee of Helsinki University Central Hospital and all patients and controls gave informed written consent. The measurements were performed 6 to 12 months after the implantation of the stimulators.

3.2 Experimental protocol

Subjects were instructed to bring their wrist to maximal dorsiflexion, or extension, for one minute at a time. The task was repeated five times with a pause of 20 seconds between each trial. The aim was to produce a sustained isometric contraction by using submaximal force. A preliminary trial was performed before the actual task trials, in which subjects extended their wrist with maximal force for comparison.

	Voltage (V)	Frequency (Hz)	Pulse width (μs)	Polarity
Patient #1				
<i>dx.</i>	3.8	150	60	bipolar
<i>sin.</i>	3.5	150	60	monopolar
Patient #2				
<i>dx.</i>	3.1	130	60	bipolar
<i>sin.</i>	3.1	130	60	bipolar
Patient #3				
<i>dx.</i>	2.3	180	60	monopolar
<i>sin.</i>	2.5	180	60	monopolar

Table 1: The patients’ DBS parameters: *dx.* refers to the right side electrode and *sin.* to the left.

The controls were asked to perform the task trial twice, first with the right and then with the left hand. The patients performed the task trial twice with their more affected hand: first, when bilateral DBS was on and, thereafter, when the stimulation was turned off. Motor disability was scored according to UPDRS III (Unified Parkinson’s Disease Rating Scale [59]) before the measurement with DBS on and after the measurement when DBS had been switched off. The UPDRS III motor score ranges from zero (no disability) to 120 (total disability) and covers the following aspects of motor performance: speech, facial expressions, rest tremor and postural tremor, rigidity, fine motor control of the hands, movements of the extremities, posture, gait, balance, and bradykinesia. The testing was performed by a trained physician.

To obtain an electromyogram of the muscles performing the motor task, a bipolar surface electrode was attached to the forearm on top of the *extensor carpi radialis* muscle. To record finger tremor related to muscle tension, an accelerometer (ADXL335 iMEMS Accelerometer, Analog Devices Inc., Norwood, MA, USA) was attached to the nail of the index finger in both hands. The accelerometers measured finger acceleration in three orthogonal directions.

To distinguish the tremor observed during wrist dorsiflexion from Parkinson’s rest tremor, we refer to the tremor type of interest as *postural tremor*. Postural tremor is observed in the fingers with static tension of the wrist extensor muscles and is found in healthy controls as well as Parkinson’s patients. To limit our study to this particular tremor type, patients with a tremor-dominant disease were excluded from the study. In addition, any patient who exhibited constant, large-amplitude tremor during the measurements had to be excluded, because the tremor signal masked the onset of the task in the electromyogram.

3.3 Data collection

3.3.1 MEG and MRI data collection

The MEG data used in this Thesis was collected for the works of Airaksinen et al. [39,56,60] between years 2010 and 2014. The MEG measurements were conducted with the 306-channel Elekta Neuromag[®] MEG device (Elekta Oy, Helsinki, Finland) in a magnetically shielded room (Euroshield, Eura, Finland) at the imaging facilities of the BioMag Laboratory (Helsinki University Central Hospital). The 306-channel MEG device comprises 102 three-channel units containing two orthogonal planar gradiometers and a magnetometer. The channel units are arranged in a helmet-shaped array that covers most of a subject's head except for the face below the level of the eyebrows.

Data were collected with a sampling frequency of 1012.5 Hz and low- and highpass filter corners at 330 and 0.03 Hz, respectively. The subjects were placed under the sensor helmet in a sitting position with their forearm resting on a pillow at the level of the waist. Patient data were collected between 6 and 12 months after the operation to rule out potential operation-related effects on brain function. The anatomical MRIs had been collected in Helsinki University Central Hospital with a 1,5 Tesla MRI system (Siemens Medical Systems).

3.3.2 Phantom measurements

Phantom measurements were conducted using bilateral Acliva PC neurostimulators (Medtronic Inc., Minneapolis, MN) embedded in a watermelon (Figure 15). Different electrode configurations were used to model different stimulation settings. For the purposes of this study, we analyzed one data set from measurements that used the bipolar configuration, a second that used the monopolar configuration, and a third measured with stimulation off. The stimulation parameters had been chosen to match those commonly used in patients: 130 Hz for stimulation frequency and 60 μ s for pulse width. To maximize the stimulation-related artefacts, higher voltage (10 V) was applied than is used to treat patients. Data were collected in the BioMag Laboratory.

3.4 Data preprocessing

3.4.1 Artefact identification

The phantom data sets were preprocessed using tSSS. Averaged spectral density was calculated for each set. The comparison between the monopolar and the bipolar configuration is depicted in Figure 16. The figure reveals a clear difference in artefact patterns: the monopolar configuration (blue) seems to produce a denser interference pattern with peaks larger in amplitude than those produced by the bipolar configuration (red). Some of the peaks, although not all, overlap: those



Figure 15: Preparations for the phantom measurements: the watermelon containing the embedded neurostimulators was placed inside the MEG helmet in a position that roughly corresponds to the position of a human subject.

appearing at 50 Hz, 100 Hz, and 150 Hz match with the powerline frequency and its harmonics, while the 130 Hz peak clearly corresponds to the DBS frequency. In addition, Figure 16 shows greater baseline noise for the monopolar configuration than for the bipolar configuration.

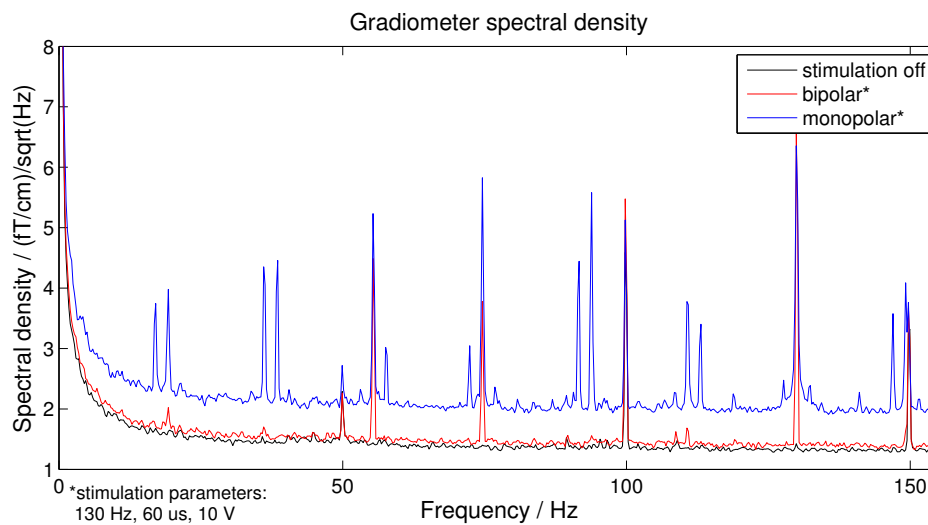


Figure 16: Comparison of artefacts produced by the monopolar (blue) and the bipolar (red) configuration: averaged gradiometer spectral density obtained from phantom measurements (data preprocessed with tSSS).

One of the patients (Patient #2 in Table 1), using the same stimulation frequency as the phantom, 130 Hz, was used as a reference to compare phantom artefacts with those observed in patients. Figure 17 illustrates the findings. Again, powerline artefacts are seen in both spectra, and the DBS peak appears at 130 Hz. Most artefactual peaks found in the patient coincide with those seen in the phantom, except for a peak at 110 Hz and smaller peaks at 95, 35, and possibly 20 Hz.

For the purposes of this study, we note that the main artefactual peaks that persist after tSSS-preprocessing are localized above 30 Hz; in other words, beyond our frequency range of interest. Furthermore, our analysis mainly concerns MEG signals that are coherent with an external signal; that is, extensor muscle EMG and finger acceleration. The coherence analysis is likely to cancel any artefactual contribution, unless the artefact spreads to the peripheral measurement, which is unlikely, especially in the case of the accelerometer. Thus, tSSS appears to provide satisfactory interference suppression for our measurements.

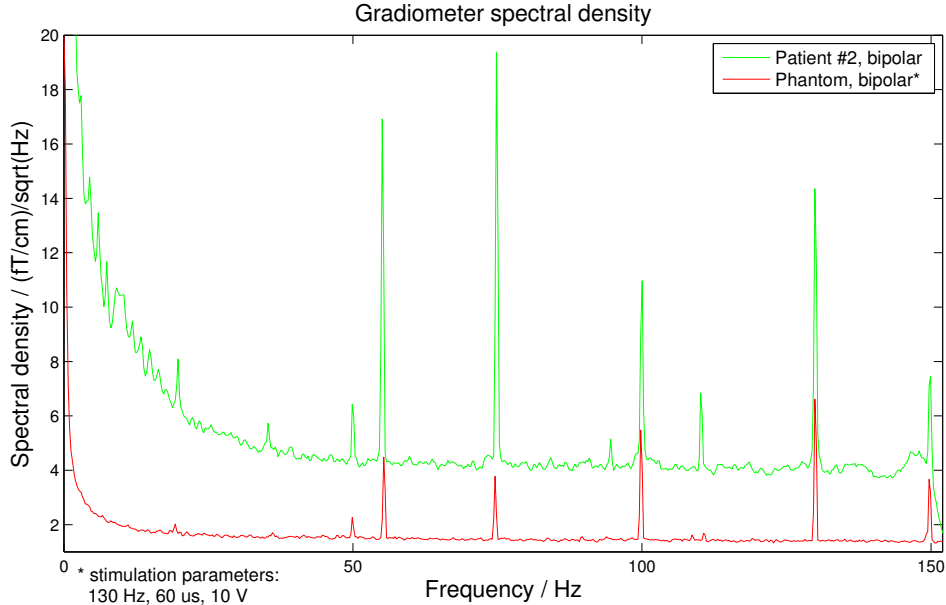


Figure 17: Comparison of artefacts produced by bipolar stimulation in phantom (red) and bilateral DBS in Patient #2 (green) (data preprocessed with tSSS). The high baseline in the patient’s spectrum at frequencies below 50 Hz derives mainly from brain activity and physiological artefacts.

3.4.2 Coregistration and MRI preprocessing

Prior to the measurements, the locations of four firmly attached head position indicator (HPI) coils and extra points were digitized in the head coordinate system defined by three digitized anatomical landmark points. Figure 18 illustrates the locations of the anatomical landmarks: the left and the right preauricular point and the nasion. Before data recording was initiated, the HPI coils were driven with

sinusoidal currents of defined frequencies, higher than the brain signals of interest, and the accompanying magnetic fields were collected for the localization of the coils.

The coil locations with respect to the MEG sensor array set the coordinate transformation between the head coordinate system and the MEG coordinates. Recently, it has become possible to track the head position continuously during the measurement [46]. All patient measurements and all but one control measurement in this Thesis employed this continuous tracking of head position.

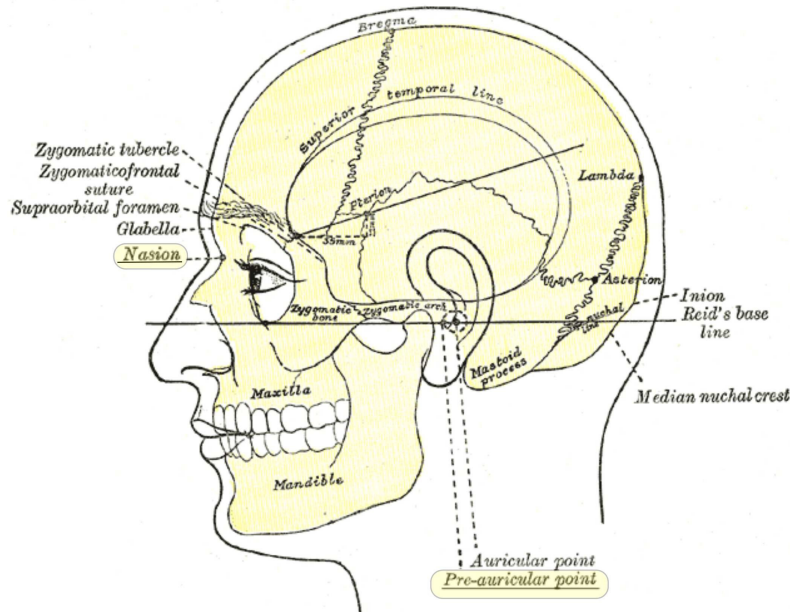


Figure 18: The location of the anatomical landmarks used to define the head coordinate system. The nasion and the left preauricular point are highlighted in the figure. Adapted from [61].

Coregistration was performed by identifying the anatomical landmarks in the MRIs and by fitting the extra points to the head surface using the MRILab software (Elekta Oy, Helsinki, Finland). The matching provided a coordinate transformation between the head coordinates and the MRI coordinates. Since a transformation from MEG to head coordinates had already been calculated, a transformation from MEG to MRI coordinates was thus available.

MRI-segmentation was performed to distinguish the brain from the surrounding tissues. To segment the control MRIs we used the FreeSurfer software (MGH, Boston, MA) [62] that performs the segmentation automatically. Minor manual corrections were made to the images after automatic segmentation. Manual segmentation was employed for patient MRIs due to poorer image quality. The Seglab software (Elekta Oy, Helsinki, Finland) was used for manual segmentation.

3.4.3 MEG data preprocessing

The MEG data obtained from the patients and the controls were preprocessed using the tSSS (Maxfilter, Elekta Oy) to suppress interfering signals caused, in particular, by DBS and the stimulation hardware, as well as external magnetic fields. We employed a correlation limit of 0.9 and a buffer length of 8 seconds. The data were inspected using the signal processing software Graph (Elekta Oy). Data segments corresponding to the task trials were manually selected according to the time points reported during the measurement, and selection was based on the visual appearance of both EMG and accelerometer signals. The segments were concatenated using Matlab (MathWorks, MA, U.S.A.) for the data analysis.

3.5 Data analysis

3.5.1 Spectrum analysis

Power spectra were calculated for the electromyograms and the accelerograms using the signal processing software Graph (Elekta Oy). The calculation utilized the Welch’s method described in Section 2.3.4. We used a window size of 4096 samples, which corresponds to a frequency resolution of approximately 0.25 Hz when considering the sampling frequency of 1012.5 Hz. The aim of the frequency spectrum analysis was to examine spectral maxima: we looked at peaks between 5 and 12 Hz associated with postural tremor as reported by Caviness et al. [54] as well as peaks at the beta band (14–30 Hz) that could be associated with CMC.

3.5.2 Sensor-level coherence

Sensor-level coherence between MEG and accelerometer signals was computed in Matlab to single out spectral maxima at the beta band (14–30 Hz). Coherence was calculated for one accelerometer channel at a time².

The beta band was inspected for coherence peaks in particular in the sensors closest to the motor cortex contralateral to the task-performing hand, that is, the sensors closest to the posterior frontal cortex. The largest peak observed at this frequency range was used to define a 6-Hz frequency band at which we would estimate source-level CMC and CKC. We refer to the frequency band used in the coherence analysis as the *coherence band*.

The coherence bands were then contrasted with the findings from the spectrum analysis. In other words, any peaks that had been observed at the beta band in the coherence analysis were compared with the coherence band and the frequency of maximum coherence. Finally, a nonparametric correlation test (Spearman’s r_s)

²We tried combining the accelerometer channels by using their Euclidean norm but noticed the resulting coherence was lower than the maximum coherence achieved with a single channel.

was performed to assess potential correlation between the postural tremor frequency and the beta band frequency of maximum coherence.

3.5.3 Source-space coherence

Source-space coherence was estimated using an LCMV beamformer (Elekta Oy). The method, entitled *dynamic imaging of coherent sources*, was first introduced for the analysis of cortico-cortical coherence [63] but can be equally applied to coherence between cortical and peripheral signals. Coherence scores were estimated for the previously defined 6-Hz coherence bands. CMC was estimated between the MEG and the EMG obtained from the task-performing arm. CKC was calculated separately for all three accelerometer channels: in Section 4 we report the largest of the obtained values. The beamformer algorithm employed a resolution of 1 Hz; that is, to obtain a coherence score over a 6-Hz band, the algorithm averaged the scores of six frequency bins.

The statistical significance of the coherence estimates was assessed using surrogate statistics following Sekihara et al. [64] (see [65] for a detailed description). The method consists of creating surrogate data by randomizing the phase information of the Fourier transformed signals, thus destroying coherence. The randomization is repeated N times (here $N = 250$), and whole-brain coherence scores are computed for each randomized set. A null distribution is obtained by arranging the maximum surrogate coherence scores assigned to each voxel into an increasing order. A voxel-specific threshold of significance is then picked from the arranged list. The threshold depends on the designated level of significance, which in our study was 99 %.

Coherence maxima were searched in the statistically thresholded data using the hot spot tool of the MRIView software (Elekta Oy). The relevance of the maxima was evaluated based on their anatomical location: only the maxima located around the central sulcus (posterior frontal and anterior parietal lobe) were considered relevant for our study. The area in question covers the primary motor and sensory cortices, respectively. The results of the beamformer analysis are presented in Section 4.4.

4 Results

4.1 Motor disability scores (UPDRS III)

Two out of three patients showed a clinically significant worsening of symptoms when DBS was turned off (Table 2). The increase in the UPDRS III motor score varied between 6 and 39 points. One patient showed a mild improvement after DBS had been switched off, corresponding to a decrease of 5 points. Since the patients were on their usual anti-Parkinsonian medication during the experiment, the changes observed in the UPDRS scores cannot be wholly attributed to the cessation of DBS. Table 3 presents the patients' upper extremity tremor profiles: Patient #1 had no rest tremor, Patient #2 had mild rest tremor with DBS on, and Patient #3 slight or infrequent rest tremor with DBS off.

Patient	DBS on	DBS off	Difference
1	18	24	+6
2	42	37	-5
3	6	45	+39

Table 2: The UPDRS III motor scores of the patients measured before and after the measurement. A positive difference between the two conditions indicates a worsening of symptoms when DBS has been switched off.

Patient	DBS on	DBS off
1	0	0
2	2	0
3	0	1

Table 3: The patients' rest tremor scores of the more affected hand (UPDRS III, item 20) measured before and after the measurement (0 = absent; 1 = slight, infrequent; 2 = mild; 3 = moderate; 4 = marked). The scores correspond to the more affected hand that was also measured for CMC and CKC.

4.2 Spectrum analysis

Examples of the averaged power spectra calculated for the EMG and the three accelerometer channels are presented in Figure 19 (controls) and Figure 20 (patients). Large individual variability was observed in the spectra. In controls, the most consistent feature was a peak between 8 and 11 Hz, observed in nine out of ten controls in both the accelerometer and the EMG spectra. One of the controls had an additional peak at 6 Hz in his right hand spectrum. There was little difference in the frequency of the peak between hands for most subjects but some showed larger variability: the largest difference between hands was 2 Hz, a significant difference considering the spectral resolution of 0.25 Hz. Three out of ten controls showed increased spectral

power between 14 and 30 Hz in one of the two hands (not observed for Control #7 in Figure 19). However, the increase from the baseline was minor compared to the peaks between 5 and 12 Hz.

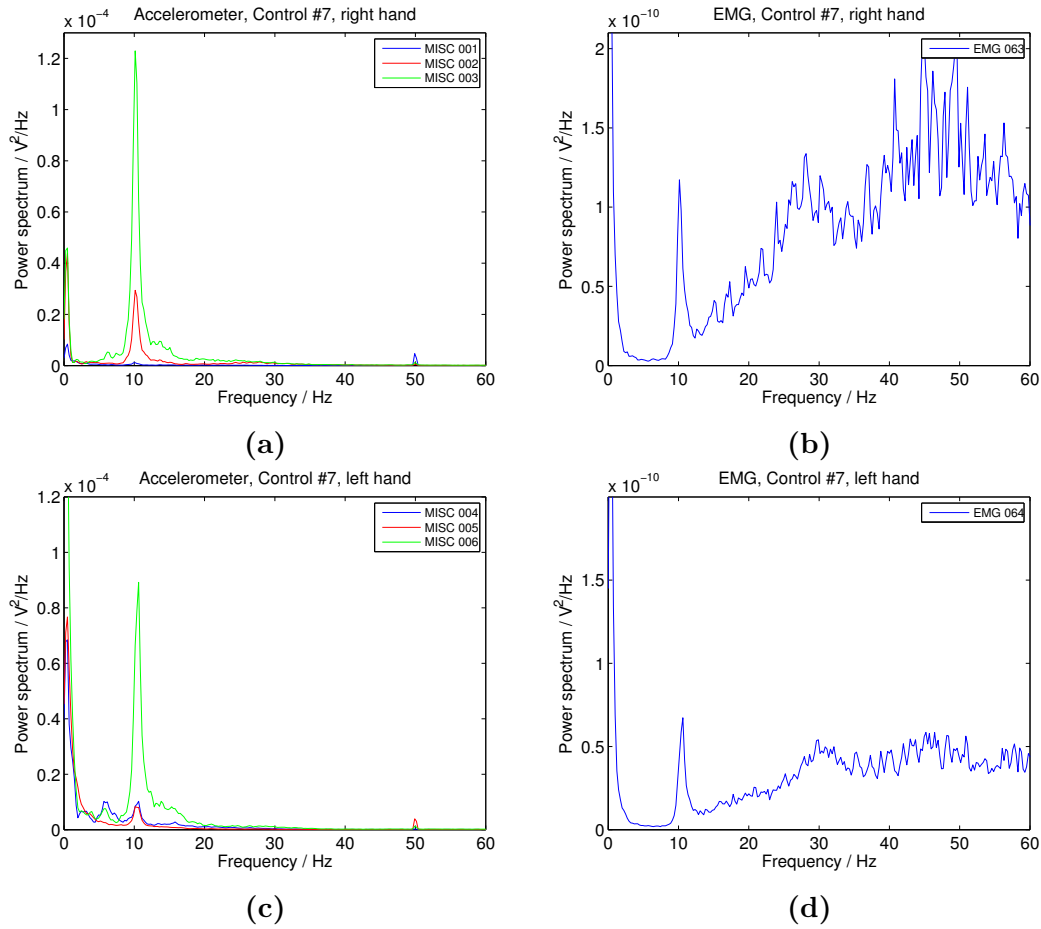


Figure 19: EMG and accelerometer power spectra obtained from Control #7 (see Table 4 for the corresponding coherence bands). Figures (a) and (b) correspond to the right hand and (c) and (d) to the left. Channels MISC 001...003 and 004...006 measure acceleration in three orthogonal directions in the right and left index finger, respectively.

For all patients, we observed a peak between 5 and 7 Hz in the accelerometer spectrum both with DBS on and off. However, the correlation between the accelerometer and the EMG spectra was poorer than for the controls and no corresponding peak was seen in the EMG spectra for two out three patients. For two out of three patients the most prominent accelerometer peak was greater in amplitude with DBS off than with DBS on, suggesting increased tremor after DBS had been switched off. The accelerometer spectra of Patients #2 and #3 showed a slight increase in spectral power at the beta band with both DBS on and off. However, the increase was relatively weak. In addition, the EMG spectrum of Patient #3 showed a more dramatic rise at the beta band with DBS off. Appendix A presents the spectra of all patients.

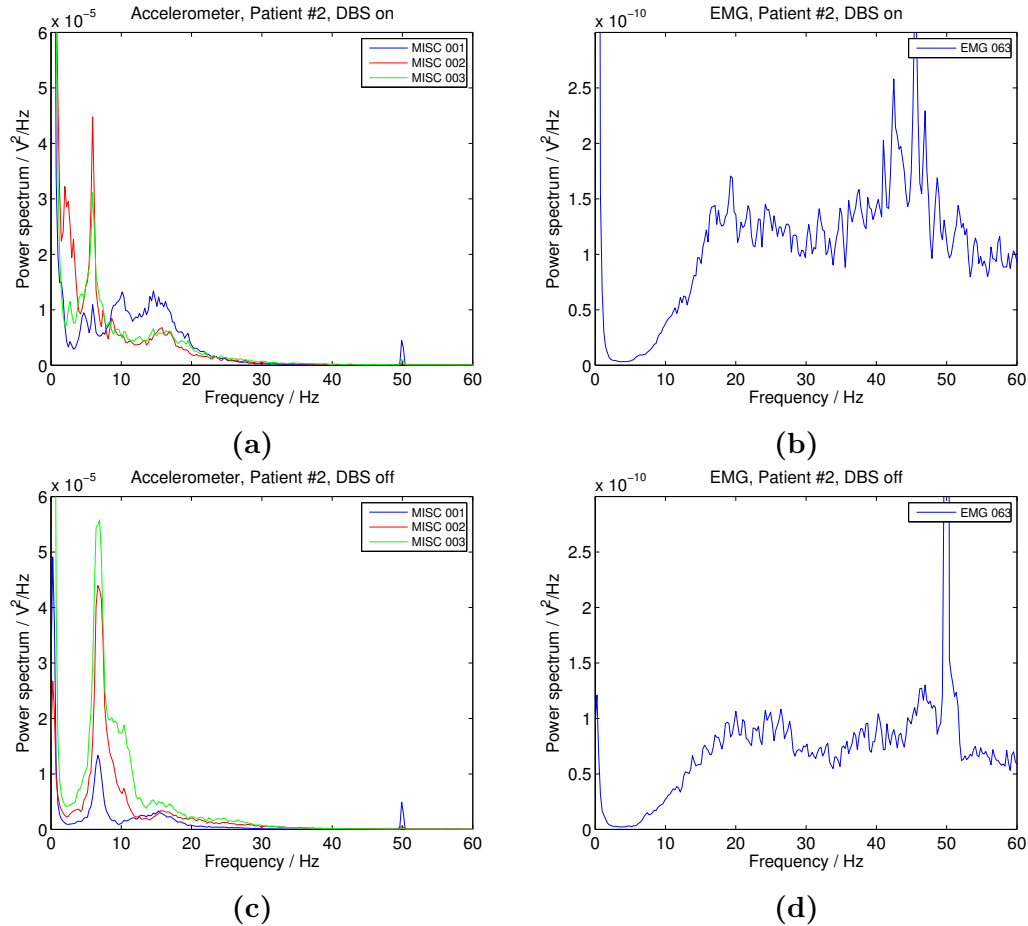


Figure 20: EMG and accelerometer power spectra obtained from Patient #2. Subfigures (a) and (b) correspond to the DBS on state while (c) and (d) correspond to the DBS off state.

When comparing tremor amplitudes between controls and patients, we noticed they were on the same order of magnitude. In fact, the average amplitude was greater in the controls than the patients. However, one control showed no postural tremor visible in the spectra. Due to the small sample size of the patient group, no statistical testing was applied to test the difference in amplitude between the groups.

4.3 Sensor-level coherence

Figure 21 illustrates the process of defining the coherence bands from sensor-level coherence spectra. The data from each patient and each control underwent the same procedure in which we selected the most prominent peak between 14 and 30 Hz. With a precision of 1 Hz this peak defined the center of the coherence band; for example, in the case of Figure 21, where the maximum is seen roughly at 16 Hz, we set the coherence band at 13–19 Hz.

The coherence bands are listed in Tables 4 and 5 for the controls and the patients,

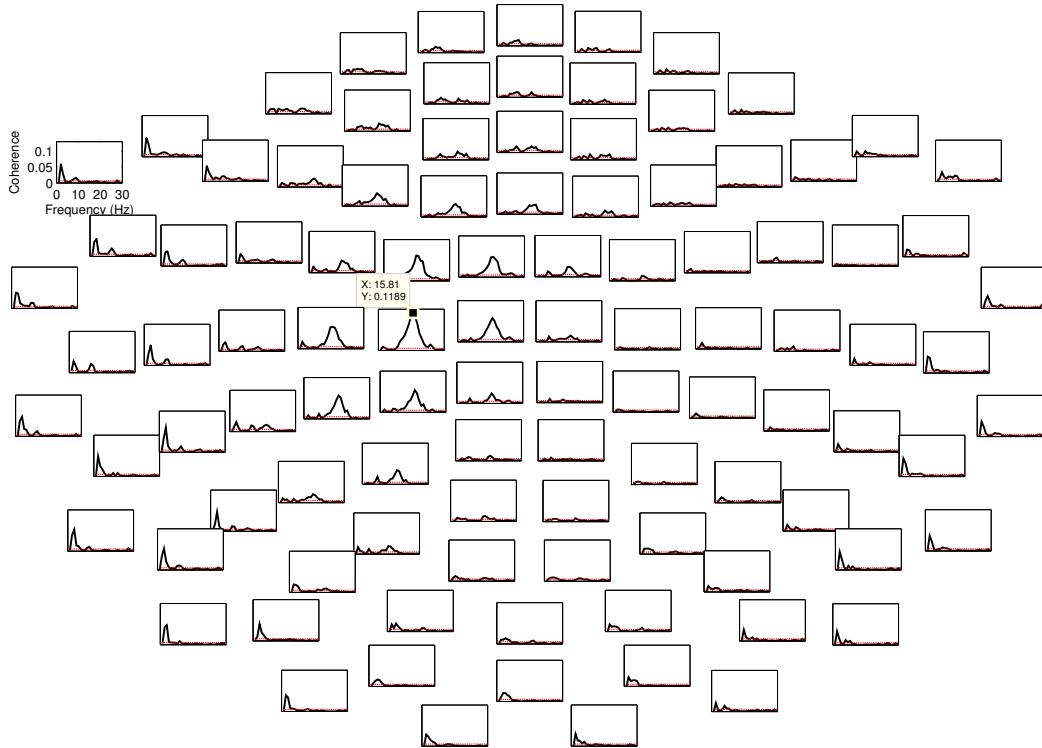


Figure 21: Sensor-level coherence results (Patient #2 with DBS on). The largest coherence peak is marked with a dot: the x -coordinate shows the frequency and the y -coordinate the coherence score. The sensors are seen from the top, the nose facing up. Orthogonal gradiometers have been combined in the computation and are presented here.

respectively. Table 4 shows that only two out of ten controls have identical coherence bands for both hands while the rest show a shift of 1 to 5 Hz. This means the coherence maximum appears at a slightly different frequency between hands. In Table 5 we note a shift in the coherence band in two out of three patients when DBS is switched off.

Control	Right (Hz)	Left (Hz)
1	20–26	21–27
2	19–25	19–25
3	19–25	18–24
4	13–19	18–24
5	22–28	20–26
6	21–27	19–25
7	23–29	24–30
8	12–18	12–18
9	15–21	12–18
10	19–25	17–23

Table 4: Coherence bands (controls). Boldface refers to Figure 19 in Section 4.2.

Patient	DBS on (Hz)	DBS off (Hz)
1	16–22	18–24
2	13–19	13–19
3	22–28	15–21

Table 5: Coherence bands (patients). The band is chosen so that it covers 6 Hz around the frequency of maximum coherence observed between 14 and 30 Hz.

When comparing the EMG and accelerometer spectra with the coherence bands, we failed to notice any clear correlation between the two. In the controls, although some of the observed increases at the beta band were localized within the subject’s coherence band, the peak intensity did not coincide with the frequency of maximum coherence. Also in the patient group the slight increases seen in the spectra at the beta band showed poor overlap with the coherence spectra. The more dramatic rise seen in the EMG spectrum of Patient #3 did not coincide with the patient’s coherence band (see Appendix A and Table 5 for reference). Thereby, we conclude that EMG or accelerometer power spectra cannot be used in determining the frequency of maximum coherence.

Finally, to see if the postural tremor frequency correlated with the sensor-level coherence frequency, we performed statistical testing: the nonparametric Spearman’s r_s showed a significant positive correlation between the tremor frequency and the frequency of maximum coherence ($r_s = 0.658$, $p = 0.003$) in controls. The correlation remained significant when patient data was added to the pool but decreased in significance ($r_s = 0.513$, $p = 0.01$), and the patient group alone showed no significant correlation. Figure 22 illustrates the observed correlation.

4.4 Source-space coherence

The results of the beamformer analysis are presented in Appendix B for the controls and Figure 23 for the patients. The figures show that the CMC and CKC maxima were located in the hemisphere contralateral to the task-performing hand at the anterior parietal/posterior frontal cortex both in patients and in controls.

The controls had a mean CKC_{max} score of 0.046 and a mean CMC_{max} score of 0.048. We performed a paired t -test to compare the means of the two measures and showed that the difference was non-significant (confidence level 95 %, $p = 0.587$). In the patients group we looked at the two conditions separately: when DBS was on the patients had a mean CKC_{max} score of 0.070 and a mean CMC_{max} score of 0.093; when DBS had been switched off, the mean scores were 0.10 and 0.13, respectively.

Thus, we observe that the patients’ average coherence scores appear higher in the DBS off condition than when DBS in on. In addition, the patients’ scores are higher than the controls’ in both conditions. In the patient group, the CMC_{max} scores appear higher than the CKC_{max} scores. However, due to the small sample size, these interpretations lack statistical power.

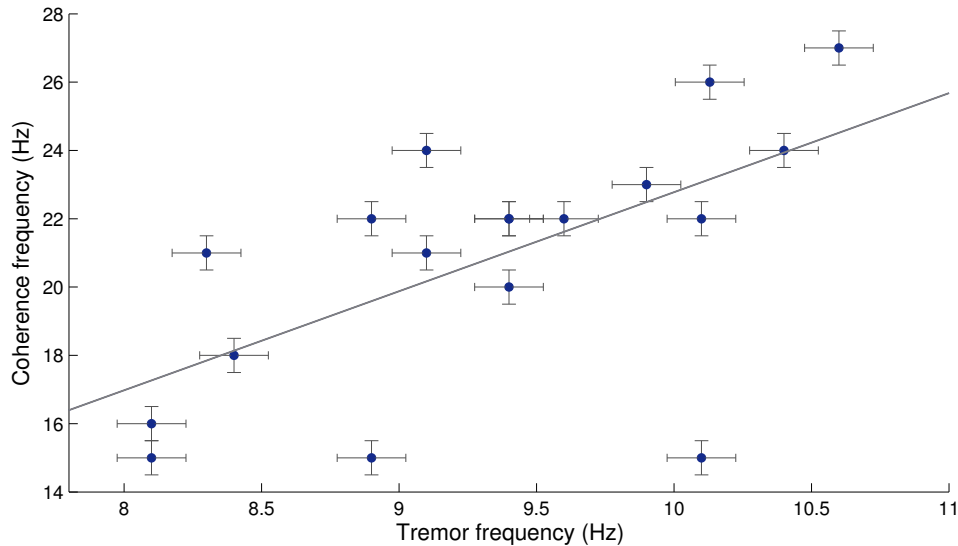


Figure 22: The correlation between the postural tremor frequency and the frequency of maximum coherence in the control group. Each control that showed significant postural tremor (nine out of ten controls) is represented by two dots (one for each hand/hemisphere). The line has been fitted using the method of least squares.

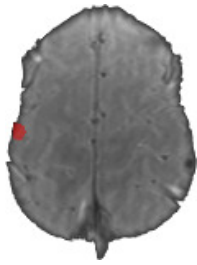
When correlating the coherence scores with the clinical state we observe that Patients #1 and #3 exhibit an increase in coherence when DBS is switched off. The scores are more than tripled for Patient #3 but less than doubled for Patient #1 (Table 6). Patient #2 shows a decrease in the coherence scores when DBS is switched off. The coherence scores are averages over a 6-Hz band, which, in addition, changed for Patients #1 and #3 between the DBS on and DBS off states. Thus, caution should be taken when comparing the scores between the two conditions. Interestingly however, the CMC and CKC show similar behavior relative to each other when DBS is switched off.

Thanks to better MRI quality, the anatomy underlying the coherence maxima can be better appreciated in controls than in patients. Although we cannot deduce the exact anatomical origin of the coherent signal from the beamformer results, coherence seems to arise in the proximity of the primary motor cortex. In Patient #2 one can easily discern the "hand knob", the omega-shaped protrusion of the primary motor cortex anterior to the central sulcus, and the coherence maxima slightly lateral to this structure. We conclude that in most cases the CKC and the CMC maxima are colocalized.

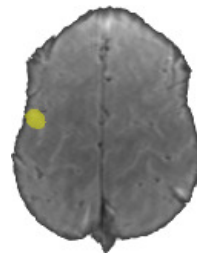
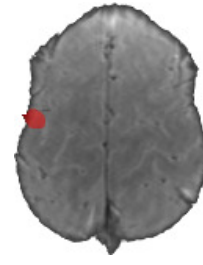
Finally, to see if larger postural tremor amplitude correlates with stronger CKC in the control group, we used the nonparametric Spearman's r_s , which showed no significant correlation ($r_s = 0.181$, $p = 0.473$). No statistical testing was applied to the patient group because of small sample size, but a corresponding scatter plot showed no indication of a linear relationship between tremor amplitude and CKC score.

Patient #1

DBS on: 16-22 Hz

 $CKC_{\max} = 0.06$  $CMC_{\max} = 0.08$

DBS off: 18-24 Hz

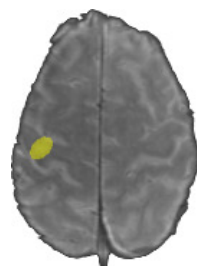
 $CKC_{\max} = 0.10$  $CMC_{\max} = 0.12$

Patient #2

DBS on: 13-19 Hz

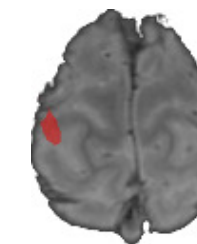
 $CKC_{\max} = 0.12$  $CMC_{\max} = 0.16$

DBS off: 13-19 Hz

 $CKC_{\max} = 0.11$  $CMC_{\max} = 0.13$

Patient #3

DBS on: 22-28 Hz

 $CKC_{\max} = 0.03$  $CMC_{\max} = 0.04$

DBS off: 15-21 Hz

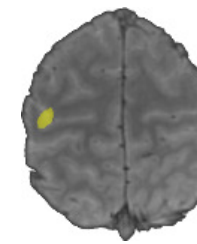
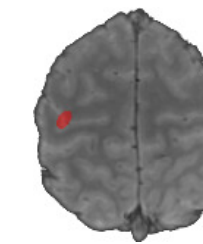
 $CKC_{\max} = 0.09$  $CMC_{\max} = 0.13$

Figure 23: The beamformer estimates of areas of maximum CMC and CKC with DBS on and DBS off superimposed on patient MRIs. The yellow/red area corresponds to the volume in which the statistically assigned top 10 % of coherence values are located. Stronger color intensity signifies greater coherence. The images are oriented so that the patient's left hemisphere is located on the left.

Patient	DBS on	DBS off	Fold change
1			
CKC_{max}	0.06	0.10	1.5
CMC_{max}	0.08	0.12	1.5
2			
CKC_{max}	0.12	0.11	0.9
CMC_{max}	0.16	0.13	0.8
3			
CKC_{max}	0.03	0.09	3.5
CMC_{max}	0.04	0.13	3.2

Table 6: Comparison of coherence maxima with DBS on and off. The fold change is calculated by dividing the DBS off -state value with the DBS on -state value.

5 Discussion

We investigated the effects of DBS in three patients with advanced PD by measuring CMC and CKC with DBS on and off. Two out of three patients showed clinically significant worsening of their motor symptoms when DBS was switched off. The third patient showed a slight decrease in the UPDRS III motor disability score indicating a mild improvement in the clinical state after DBS had been switched off. It is possible that the antiparkinsonian medication taken right before the measurement clouded to some extent the clinical effect of DBS for this patient. Also, some symptoms, such as dyskinesias, take a longer time to manifest themselves after turning off the stimulation and were hence unlikely to appear during the measurement.

Examining the accelerometer spectra, we noticed a peak in all patients and in nine out of ten controls between 5 and 11 Hz indicating the presence of small-amplitude postural tremor in both groups. Average tremor amplitude was on the same order of magnitude in the patient and the control group; earlier findings support this observation [66]. Our experimental protocol did not include explicit assessment of postural tremor, but the prevalence of tremor peaks in the control spectra suggests the tremor would not have been clinically visible in all subjects. Caviness et al. [54] have also reported spectral peaks at tremor frequencies in healthy subjects with no visible postural tremor.

We observed discrepancy between EMG and accelerometer spectra especially in the patient group: the postural tremor peak was not present in all EMG spectra. Our findings contrast here with Caviness et al. [54] who reported in their examination of EMG power spectra a prominent peak between 5 and 12 Hz; however, their data show large variability. The poor correlation between the EMG and the accelerometer spectra could be due to different noise profiles in the accelerometer and the EMG signal as well as the potentially inconsistent placement of the EMG electrodes across patients. In addition, the postural tremor observed in patients could be produced by muscles other than those targeted for EMG (e.g. the small muscles of the hand). The inconsistencies in the EMG spectra support the use of sensitive accelerometers in the study of tremor.

We detected a difference in the tremor frequency range between groups, 5–7 Hz for the patients and 8–11 Hz for the controls. In addition, we noticed a linear relationship between the tremor frequency and the frequency of maximum coherence in the control group but not in the patient group; however, the small number of patients inevitably reduces the statistical value of the latter observation. Such differences between groups suggest the postural tremor of PD patients may exhibit pathological features. However, considering that Caviness et al., who also measured postural tremor frequency in PD patients and in healthy controls, did not report any difference in frequency between groups [54], we conclude that further studies are required to investigate whether the differences observed in our study are actually due to a difference in aetiology.

The EMG and accelerometer spectra did not contain peaks between 14 and 30 Hz.

Some increase in spectral power was observed at the beta band but the activity was distributed and relatively weak in comparison with the peaks below 11 Hz. Moreover, we did not observe any consistent increase in spectral power between 12 and 18 Hz, a finding reported by Caviness et al. [54] for PD patients with visible postural tremor. In contrast to Caviness et al., we did not classify the patients according to their postural tremor amplitude and therefore cannot directly compare the findings. Nevertheless, we concluded that power spectrum analysis of EMG/acceleration data does not enable the determination of the beta band frequencies that show greatest coherence with a cortical signal.

The results of the coherence analysis are in agreement with earlier findings by Conway et al. [12] and Salenius et al. [52], showing statistically significant corticomuscular coherence at the beta band (14–30 Hz) in sustained muscle contraction. Like previous studies, our study shows large individual variation in coherence frequency and magnitude. Unlike Salenius et al. [13], we did not test for the effects of medication; however, all our patients were on anti-Parkinsonian medication during the experiment, which may explain significant coherence both with DBS on and with DBS off.

We observed that coherence scores increased when DBS was switched off in the patients who showed a simultaneous worsening of clinical symptoms; moreover, the increase correlated with the change in the UPDRS III score of motor dysfunction. Airaksinen et al. [56] have shown that the clinical tremor profile of the patient may affect coherence findings: having divided the patients into akinetic-rigid and tremor-dominant groups, they observed that the majority of the akinetic-rigid patients showed significant coherence in both conditions, while none of the tremor-dominants showed similar behavior, having significant coherence only in one of the two or none of the two conditions. Considering that our patients represented the akinetic-rigid variant of PD, having rest tremor scores that vary from absent to mild, our observations are in line with their results.

Studies on Parkinsonian rest tremor have demonstrated that a tremorous episode is associated with increased CMC at the tremor frequency and its first harmonic along with a simultaneous decrease in cortical beta power possibly similar to the beta desynchronization associated with voluntary repetitive movements [67]. These tremor-induced changes in beta power could explain the observations by Park et al. [55] who detected increased beta band coherence with DBS on for the hand in which DBS alleviated the tremor. Unpublished results by Airaksinen et al. [56] support the idea that large-amplitude tremor correlates negatively with beta band CMC. Therefore, researchers should be cautious when attributing increases in beta band coherence to a direct DBS effect in situations in which total hand movement has been simultaneously decreased, as in Park et al. [55].

Rest tremor generation has been studied by correlating direct measurements in the STN with motor cortex and muscle activity [67]. No comparable studies exist on the nature of postural tremor. Therefore, it is unclear whether the Parkinsonian postural tremor is phenomenologically different from the so-called physiological tremor.

Direct measurements at the level of the basal ganglia would be required to increase our understanding on the matter. The phenomenological connection between postural tremor and beta band CMC/CKC also requires further clarification. The linear relationship between the tremor frequency and the coherence frequency in the control group suggests a connection between the two; yet, no linear correlation was observed between tremor amplitude and CKC score.

The interpretation of the coherence scores is complicated by the fact that the scores are averages over a 6-Hz band. The averaging improves the reliability of source localization but may produce a lower score than would be achieved with a narrower band. In future studies, one could use beamformer to first locate the voxel of maximum coherence and then calculate the coherence spectrum for the source-signal of this voxel to avoid averaging errors. Here, because of the variability in the frequency of maximum coherence and the distribution of coherence across the beta band between individuals and even within individuals when DBS is switched off, it is unclear to what extent the coherence scores can be compared between individuals or between the DBS states. Moreover, the frequency of maximum coherence was defined here manually by the researcher from the sensor-level coherence plots: a more standardized method should be developed to improve comparability between studies.

The beamforming results indicate that CMC and CKC maxima colocalize at the cortex in the proximity of the central sulcus. The variability in the results makes it impossible to determine whether the coherent cortical signal is purely of motor origin or if somatosensory cortices participate in the process. Even if the primary motor cortex was the primary source of the coherent signal, sensory feedback from the primary somatosensory cortex, located in the postcentral gyrus, can be implicated in the process [58]. It should be remembered that coherence maxima shown in Section 4.4 contain inaccuracy due to the fitting errors of the coregistration process and noise that inevitably affects the results of the beamforming procedure.

Provided that the small-amplitude postural tremor of the hand exhibits a pathological frequency shift in PD, postural tremor frequency could be used as a parameter for PD pathology. Since, unlike rest tremor, postural tremor is widely present in the healthy population, comparisons between patients and healthy controls could provide novel information on the pathological mechanisms that underlie the disease. Moreover, slight postural tremor is easily measurable by simple accelerometry. However, better characterization of the tremor types present in PD should be attained before drawing conclusions on the utility of accelerometer data. Furthermore, studies on the involvement of the motor cortex-basal ganglia network in the generation of postural tremor, similar to what has been achieved in the context of rest tremor [67, 68], would be necessary for obtaining a profound understanding of the phenomenon. It has been suggested that power increases at the rest tremor frequency in the STN be used as a feedback signal for DBS [67]: if such methods are to be implemented, neural oscillations related to postural tremor generation should be considered a potential confounding factor.

6 Conclusion

We studied three patients with advanced PD and ten healthy controls with MEG to elucidate the effects of DBS on cortical oscillations and, in particular, coherence between the cortex and the musculature. Our results demonstrated statistically significant CMC and CKC between 14 and 30 Hz in all subjects with static wrist extension. CMC and CKC maxima colocalized in the proximity of the central sulcus close to the cortical hand regions. The coherence scores correlated positively with changes in clinical motor scores when DBS was switched off.

Accelerometer power spectra showed that small-amplitude postural tremor is widely present in healthy individuals and not only in individuals affected with Parkinson's disease. The tremor frequency varied between 5–7 Hz for the patients and 8–11 Hz for the controls. We did not observe any spectral peaks at the beta band that would have clearly coincided with the corresponding frequency of maximum coherence. Interestingly, the tremor frequency correlated positively with the frequency of maximum coherence in the control group.

This is the first study to measure CKC in unison with CMC in patients with PD and in healthy subjects. We show that CKC coexists with CMC and produces a coherence score of similar magnitude at the beta band in sustained muscle contraction. As a result, we introduce a novel tool for the study of motor function in PD that enables direct comparison between patients and healthy controls.

References

- [1] L. M. de Lau and M. M. Breteler, “Epidemiology of Parkinson’s disease,” *The Lancet Neurology*, vol. 5, pp. 525–535, June 2006.
- [2] W. Poewe, “Treatments for Parkinson disease — past achievements and current clinical needs,” *Neurology*, vol. 72, no. 7 Suppl, pp. S65–73, 2009.
- [3] A. L. Benabid, P. Pollak, A. Louveau, S. Henry, and J. de Rougemont, “Combined (thalamotomy and stimulation) stereotactic surgery of the VIM thalamic nucleus for bilateral Parkinson disease.,” *Applied Neurophysiology*, vol. 50, no. 1-6, pp. 344–346, 1987.
- [4] S. J. Groiss, L. Wojtecki, M. Sudmeyer, and A. Schnitzler, “Deep brain stimulation in Parkinson’s disease,” *Therapeutic Advances in Neurological Disorders*, vol. 2, pp. 20–28, Nov. 2009.
- [5] M. Zibetti, A. Merola, L. Rizzi, V. Ricchi, S. Angrisano, C. Azzaro, C. A. Artusi, N. Arduino, A. Marchisio, M. Lanotte, M. Rizzone, and L. Lopiano, “Beyond nine years of continuous subthalamic nucleus deep brain stimulation in Parkinson’s disease,” *Movement Disorders*, vol. 26, no. 13, p. 2327–2334, 2011.
- [6] M. C. Rodriguez-Oroz, E. Moro, and P. Krack, “Long-term outcomes of surgical therapies for Parkinson’s disease,” *Movement Disorders*, vol. 27, no. 14, p. 1718–1728, 2012.
- [7] A. Schnitzler and J. Gross, “Normal and pathological oscillatory communication in the brain,” *Nature Reviews Neuroscience*, vol. 6, pp. 285–296, Apr. 2005.
- [8] P. Brown, A. Oliviero, P. Mazzone, A. Insola, P. Tonali, and V. Di Lazzaro, “Dopamine dependency of oscillations between subthalamic nucleus and pallidum in Parkinson’s disease.,” *Journal of Neuroscience*, vol. 21, no. 3, pp. 1033–1038, 2001.
- [9] A. A. Kühn, F. Kempf, C. Brücke, L. G. Doyle, I. Martinez-Torres, A. Pogosyan, T. Trottenberg, A. Kupsch, G.-H. Schneider, M. I. Hariz, W. Vandenberghe, B. Nuttin, and P. Brown, “High-frequency stimulation of the subthalamic nucleus suppresses oscillatory β activity in patients with Parkinson’s disease in parallel with improvement in motor performance,” *The Journal of Neuroscience*, vol. 28, pp. 6165–6173, June 2008.
- [10] W. Penfield, “Mechanisms of voluntary movement,” *Brain: a journal of neurology*, vol. 77, no. 1, pp. 1–17, 1954.
- [11] E. Heinrichs-Graham, T. W. Wilson, P. M. Santamaria, S. K. Heithoff, D. Torres-Russotto, J. A. L. Hutter-Saunders, K. A. Estes, J. L. Meza, R. L. Mosley, and H. E. Gendelman, “Neuromagnetic evidence of abnormal

- movement-related beta desynchronization in Parkinson's disease," *Cerebral Cortex*, May 2013.
- [12] B. A. Conway, D. M. Halliday, S. F. Farmer, U. Shahani, P. Maas, A. I. Weir, and J. R. Rosenberg, "Synchronization between motor cortex and spinal motoneuronal pool during the performance of a maintained motor task in man," *The Journal of Physiology*, vol. 489, pp. 917–924, Dec. 1995.
- [13] S. Salenius, S. Avikainen, S. Kaakkola, R. Hari, and P. Brown, "Defective cortical drive to muscle in Parkinson's disease and its improvement with levodopa," *Brain: a journal of neurology*, vol. 125, pp. 491–500, Mar. 2002.
- [14] S. Taulu and J. Simola, "Spatiotemporal signal space separation method for rejecting nearby interference in MEG measurements," *Physics in Medicine and Biology*, vol. 51, p. 1759, Apr. 2006.
- [15] C. M. Tanner and S. M. Goldman, "Epidemiology of Parkinson's disease," *Neurologic Clinics*, vol. 14, pp. 317–335, May 1996.
- [16] E. Pekkonen, "Syväaivostimulaatio neurologisissa sairauksissa," *Duodecim*, vol. 129, pp. 481–488, May 2013.
- [17] D. Longo, D. Kasper, J. Jameson, A. Fauci, S. Hauser, and J. Loscalzo, *Harrison's principles of internal medicine*, vol. 18. USA: The McGraw-Hill Companies, 2008.
- [18] S. Kaakkola, "Parkinsonin tauti," *Lääketieteellinen Aikakauskirja Duodecim*, vol. 128, no. 2, pp. 167–170, 2012.
- [19] S. Soinila, M. Kaste, and H. Somer, *Neurologia*, vol. 2. Helsinki, Finland: Kustannus Oy Duodecim, 2006.
- [20] G. Deuschl, P. Bain, and M. Brin, "Consensus statement of the movement disorder society on tremor," *Movement Disorders*, vol. 13, no. 3, p. 2–23, 1998.
- [21] M. F. Bear, B. W. Connors, and M. A. Paradiso, *Neuroscience: Exploring the Brain*. Lippincott Williams & Wilkins, 2nd ed., 2001.
- [22] L. M. Ward, "Synchronous neural oscillations and cognitive processes," *Trends in Cognitive Sciences*, vol. 7, pp. 553–559, Dec. 2003.
- [23] C. Gray, "The temporal correlation hypothesis of visual feature integration: still alive and well," *Neuron*, vol. 24, no. September, pp. 31–47, 1999.
- [24] M. T. Jurkiewicz, W. C. Gaetz, A. C. Bostan, and D. Cheyne, "Post-movement beta rebound is generated in motor cortex: evidence from neuromagnetic recordings," *NeuroImage*, vol. 32, pp. 1281–1289, Sept. 2006.

- [25] W. D. Hutchison, J. O. Dostrovsky, J. R. Walters, R. Courtemanche, T. Boraud, J. Goldberg, and P. Brown, “Neuronal oscillations in the basal ganglia and movement disorders: Evidence from whole animal and human recordings,” *The Journal of Neuroscience*, vol. 24, pp. 9240–9243, Oct. 2004.
- [26] J. L. Vitek, “Deep brain stimulation for Parkinson’s disease,” *Stereotactic and Functional Neurosurgery*, vol. 78, no. 3-4, pp. 119–131, 2002.
- [27] S. K. Kalia, T. Sankar, and A. M. Lozano, “Deep brain stimulation for Parkinson’s disease and other movement disorders:,” *Current Opinion in Neurology*, vol. 26, pp. 374–380, Aug. 2013.
- [28] W. Schuepbach, J. Rau, K. Knudsen, J. Volkmann, P. Krack, L. Timmermann, T. Hälbig, H. Hesekamp, S. Navarro, N. Meier, D. Falk, M. Mehdorn, S. Paschen, M. Maarouf, M. Barbe, G. Fink, A. Kupsch, D. Gruber, G.-H. Schneider, E. Seigneuret, A. Kistner, P. Chaynes, F. Ory-Magne, C. Brefel Courbon, J. Vesper, A. Schnitzler, L. Wojtecki, J.-L. Houeto, B. Bataille, D. Maltête, P. Damier, S. Raoul, F. Sixel-Doering, D. Hellwig, A. Gharabaghi, R. Krüger, M. Pinsker, F. Amtage, J.-M. Régis, T. Witjas, S. Thobois, P. Mertens, M. Kloss, A. Hartmann, W. Oertel, B. Post, H. Speelman, Y. Agid, C. Schade-Brittinger, and G. Deuschl, “Neurostimulation for Parkinson’s disease with early motor complications,” *New England Journal of Medicine*, vol. 368, no. 7, pp. 610–622, 2013.
- [29] A. E. Lang, J.-L. Houeto, P. Krack, C. Kubu, K. E. Lyons, E. Moro, W. Ondo, R. Pahwa, W. Poewe, A. I. Tröster, R. Uitti, and V. Voon, “Deep brain stimulation: Preoperative issues,” *Movement Disorders*, vol. 21, no. 14, p. 171–196, 2006.
- [30] A. E. Lang and H. Widner, “Deep brain stimulation for Parkinson’s disease: Patient selection and evaluation,” *Movement Disorders*, vol. 17, no. 3, pp. 94–101, 2002.
- [31] J. Volkmann, N. Allert, J. Voges, V. Sturm, A. Schnitzler, and H.-J. Freund, “Long-term results of bilateral pallidal stimulation in Parkinson’s disease,” *Annals of Neurology*, vol. 55, no. 6, p. 871–875, 2004.
- [32] J. Volkmann, N. Allert, J. Voges, P. H. Weiss, H.-J. Freund, and V. Sturm, “Safety and efficacy of pallidal or subthalamic nucleus stimulation in advanced PD,” *Neurology*, vol. 56, pp. 548–551, Feb. 2001.
- [33] “Synapse deep brain stimulation.” http://www.synaptix.be/dbstherapy/dbs_therapy.php, 2012. Accessed March 20, 2014.
- [34] M. L. Kringelbach, N. Jenkinson, S. L. F. Owen, and T. Z. Aziz, “Translational principles of deep brain stimulation,” *Nature Reviews Neuroscience*, vol. 8, pp. 623–635, Aug. 2007.

- [35] J. M. Bronstein, M. Tagliati, R. L. Alterman, A. M. Lozano, J. Volkmann, A. Stefani, F. B. Horak, M. S. Okun, K. D. Foote, P. Krack, R. Pahwa, J. M. Henderson, M. I. Hariz, R. A. Bakay, A. Rezai, J. Marks, William J, E. Moro, J. L. Vitek, F. M. Weaver, R. E. Gross, and M. R. DeLong, “Deep brain stimulation for Parkinson disease: an expert consensus and review of key issues,” *Archives of neurology*, vol. 68, p. 165, Feb. 2011.
- [36] “Medtronic: Lead kit for deep brain stimulation.” http://professional.medtronic.com/wcm/groups/mdtcom_sg/@mdt/@neuro/documents/documents/dbs-1d3387-9-impman1.pdf, 1998. Accessed May 20, 2014.
- [37] C. C. McIntyre, S. Mori, D. L. Sherman, N. V. Thakor, and J. L. Vitek, “Electric field and stimulating influence generated by deep brain stimulation of the subthalamic nucleus,” *Clinical neurophysiology: official journal of the International Federation of Clinical Neurophysiology*, vol. 115, pp. 589–595, Mar. 2004.
- [38] T. Hashimoto, C. M. Elder, M. S. Okun, S. K. Patrick, and J. L. Vitek, “Stimulation of the subthalamic nucleus changes the firing pattern of pallidal neurons,” *The Journal of Neuroscience*, vol. 23, pp. 1916–1923, Mar. 2003.
- [39] K. Airaksinen, A. Butorina, E. Pekkonen, J. Nurminen, S. Taulu, A. Ahonen, A. Schnitzler, and J. P. Mäkelä, “Somatomotor mu rhythm amplitude correlates with rigidity during deep brain stimulation in Parkinsonian patients,” *Clinical Neurophysiology*, vol. 123, no. 10, pp. 2010–2017, 2012.
- [40] M. Hämäläinen, R. Hari, R. Ilmoniemi, J. Knuutila, and O. Lounasmaa, “Magnetoencephalography — theory, instrumentation, and applications to noninvasive studies of the working human brain,” *Reviews of Modern Physics*, vol. 65, no. 2, pp. 414–497, 1993.
- [41] L. Parkkonen, *Expanding the applicability of magnetoencephalography*. PhD thesis, Helsinki University of Technology, 2009.
- [42] S. Murakami and Y. Okada, “Contributions of principal neocortical neurons to magnetoencephalography and electroencephalography signals,” *The Journal of Physiology*, vol. 575, pp. 925–936, Sept. 2006.
- [43] Hansen, P., Kringelbach, M., and Salmelin, R., *MEG: An Introduction to Methods*. New York: Oxford University Press, 2010.
- [44] J. Nurminen, *The magnetostatic multipole expansion in biomagnetism: applications and implications*. PhD thesis, Aalto University School of Science, 2014.
- [45] S. Taulu, *Processing of weak magnetic multichannel signals: the signal space separation method*. PhD thesis, Helsinki University of Technology, 2008.

- [46] S. Taulu and M. Kajola, "Presentation of electromagnetic multichannel data: The signal space separation method," *Journal of Applied Physics*, vol. 97, p. 124905, June 2005.
- [47] M. Hämäläinen and J. Sarvas, "Realistic conductivity geometry model of the human head for interpretation of neuromagnetic data," *IEEE Transactions on Biomedical Engineering*, vol. 36, no. 2, pp. 165–171, 1989.
- [48] H. von Helmholtz, "Ueber einige gesetze der vertheilung elektrischer strome in körperlichen leitern, mit anwendung auf die thierischelektrischen versuche.," *Annual Review of Physical Chemistry*, vol. 89, pp. 211–233 and 353–377, 1853.
- [49] B. Van Veen, W. Van Drongelen, M. Yuchtman, and A. Suzuki, "Localization of brain electrical activity via linearly constrained minimum variance spatial filtering," *IEEE Transactions on Biomedical Engineering*, vol. 44, no. 9, pp. 867–880, 1997.
- [50] A. Hillebrand and G. R. Barnes, "Beamformer analysis of MEG data," *International Review of Neurobiology*, vol. 68, pp. 149–171, 2005.
- [51] "Programming tutorial: implementing another matlab-based filter." http://www.bci2000.org/wiki/index.php/Programming_Tutorial:Implementing_another_Matlab-based_Filter, 2009. Accessed February 12, 2014.
- [52] S. Salenius, K. Portin, M. Kajola, R. Salmelin, and R. Hari, "Cortical control of human motoneuron firing during isometric contraction," *Journal of Neurophysiology*, vol. 77, pp. 3401–3405, June 1997.
- [53] T. Mima and M. Hallett, "Corticomuscular coherence: a review," *Journal of Clinical Neurophysiology*, vol. 16, p. 501, Nov. 1999.
- [54] J. N. Caviness, H. A. Shill, M. N. Sabbagh, V. G. Evidente, J. L. Hernandez, and C. H. Adler, "Corticomuscular coherence is increased in the small postural tremor of Parkinson's disease," *Movement Disorders*, vol. 21, no. 4, p. 492–499, 2006.
- [55] H. Park, J. S. Kim, S. H. Paek, B. S. Jeon, J. Y. Lee, and C. K. Chung, "Corticomuscular coherence increases with tremor improvement after deep brain stimulation in Parkinson's disease," *Neuroreport*, vol. 20, pp. 1444–1449, Oct. 2009.
- [56] K. Airaksinen, J. Mäkelä, J. Luoma, S. Taulu, A. Ahonen, and E. Pekkonen, "Cortico-muscular coherence in advanced Parkinson's disease with deep brain stimulation," *in press*.
- [57] M. Bourguignon, X. De Tiège, M. O. de Beeck, B. Pirotte, P. Van Bogaert, S. Goldman, R. Hari, and V. Jousmäki, "Functional motor-cortex mapping using corticokinematic coherence," *NeuroImage*, vol. 55, pp. 1475–1479, Apr. 2011.

- [58] H. Piitulainen, M. Bourguignon, X. De Tiège, R. Hari, and V. Jousmäki, “Coherence between magnetoencephalography and hand-action-related acceleration, force, pressure, and electromyogram,” *NeuroImage*, vol. 72, no. 0, pp. 83–90, 2013.
- [59] C. G. Goetz, B. C. Tilley, S. R. Shaftman, G. T. Stebbins, S. Fahn, P. Martinez-Martin, W. Poewe, C. Sampaio, M. B. Stern, R. Dodel, B. Dubois, R. Holloway, J. Jankovic, J. Kulisevsky, A. E. Lang, A. Lees, S. Leurgans, P. A. LeWitt, D. Nyenhuis, C. W. Olanow, O. Rascol, A. Schrag, J. A. Teresi, J. J. van Hilten, and N. LaPelle, “Movement disorder society-sponsored revision of the Unified Parkinson’s Disease Rating Scale (MDS-UPDRS): scale presentation and clinimetric testing results,” *Movement Disorders*, vol. 23, pp. 2129–2170, Nov. 2008.
- [60] K. Airaksinen, J. P. Mäkelä, S. Taulu, A. Ahonen, J. Nurminen, A. Schnitzler, and E. Pekkonen, “Effects of DBS on auditory and somatosensory processing in Parkinson’s disease,” *Human Brain Mapping*, vol. 32, no. 7, pp. 1091–1099, 2011.
- [61] “EEG scalp current density and source current modelling notes.” http://psdlw.users.sourceforge.net/career/dweber_docs/eeg_scd.html, 2009. Accessed March 20, 2014.
- [62] “Freesurfer image analysis suite.” <http://surfer.nmr.mgh.harvard.edu/>, 2012. Accessed May 22, 2011.
- [63] J. Gross, J. Kujala, M. Hämäläinen, L. Timmermann, A. Schnitzler, and R. Salmelin, “Dynamic imaging of coherent sources: Studying neural interactions in the human brain,” *Proceedings of the National Academy of Sciences of the United States of America*, vol. 98, pp. 694–699, Jan. 2001.
- [64] K. Sekihara, J. Owen, S. Trisno, and S. Nagarajan, “Removal of spurious coherence in MEG source-space coherence analysis,” *IEEE Transactions on Biomedical Engineering*, vol. 58, no. 11, pp. 3121–3129, 2011.
- [65] J. Luoma, “MEG coherence estimates — simulation based sensitivity analysis and application to patient data,” Master’s thesis, Aalto University School of Science, 2014.
- [66] B. Scanlon, B. Levin, D. Nation, H. Katzen, A. Guevara-Salcedo, C. Singer, and S. Papapetropoulos, “An accelerometry-based study of lower and upper limb tremor in Parkinson’s disease,” *Archives of Neurology*, vol. 20, no. 6, pp. 827–830, 2013.
- [67] J. Hirschmann, C. J. Hartmann, M. Butz, N. Hoogenboom, T. E. Özkurt, S. Elben, J. Vesper, L. Wojtecki, and A. Schnitzler, “A direct relationship between oscillatory subthalamic nucleus–cortex coupling and rest tremor in Parkinson’s disease,” *Brain*, vol. 136, no. 12, pp. 3659–3670, 2013.

- [68] L. Timmermann, J. Gross, M. Dirks, J. Volkmann, H.-J. Freund, and A. Schnitzler, “The cerebral oscillatory network of Parkinsonian resting tremor,” *Brain*, vol. 126, pp. 199–212, Jan. 2002.

Appendices

A Patients: power spectra

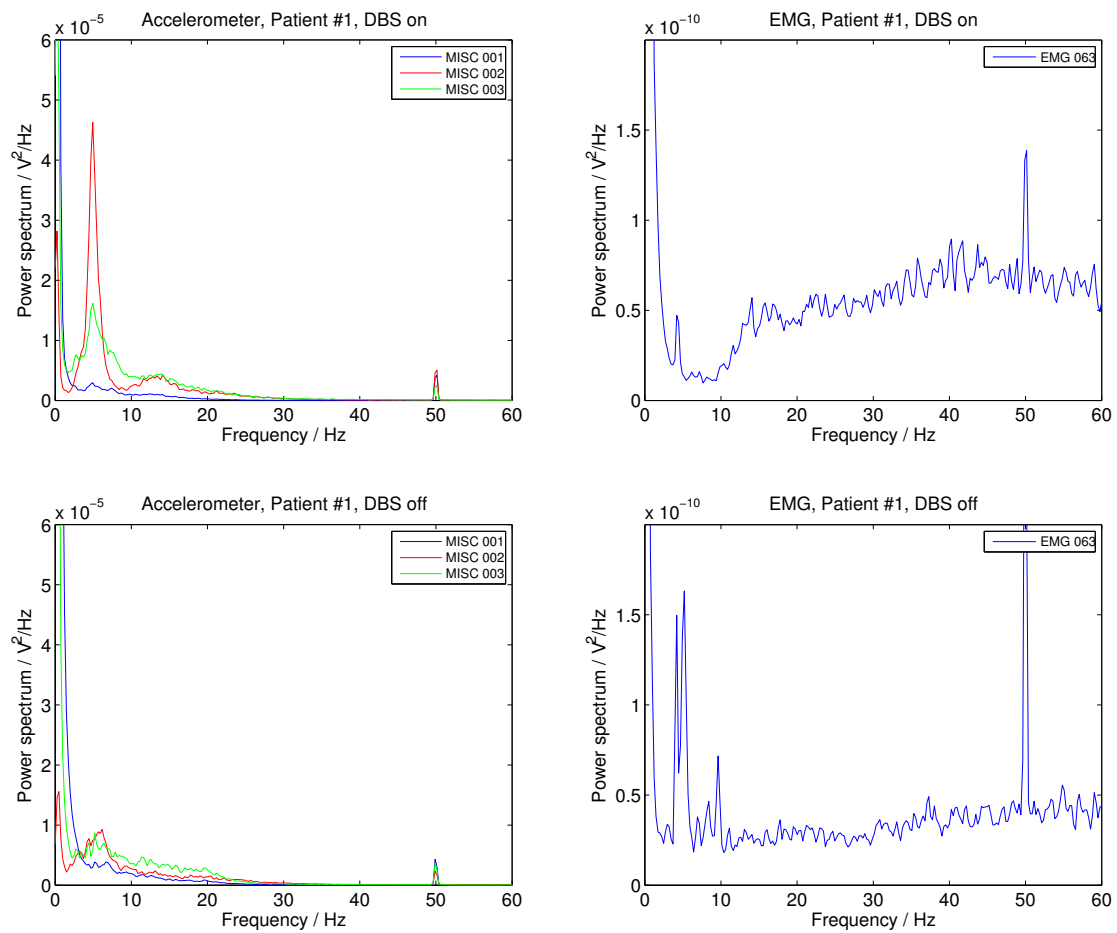


Figure 24: Power spectra: Patient #1.

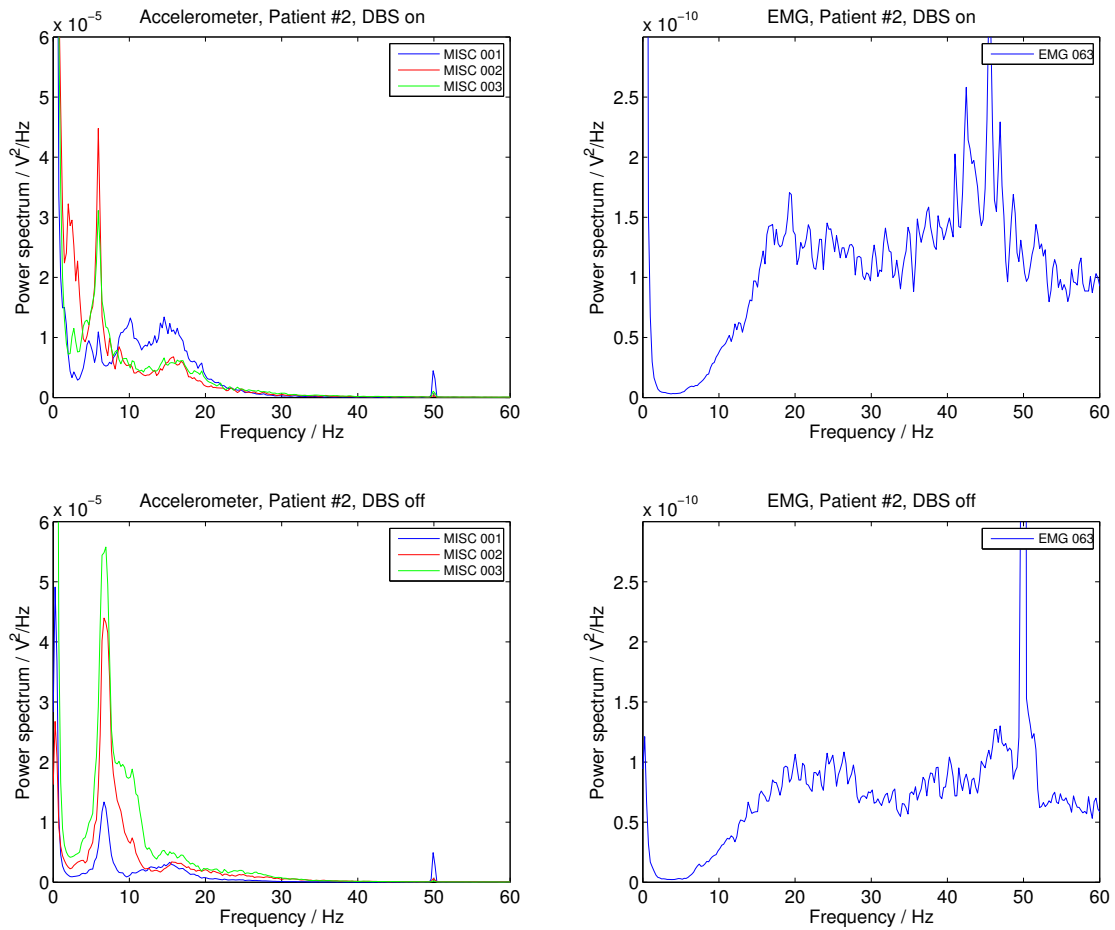


Figure 25: Power spectra: Patient #2.

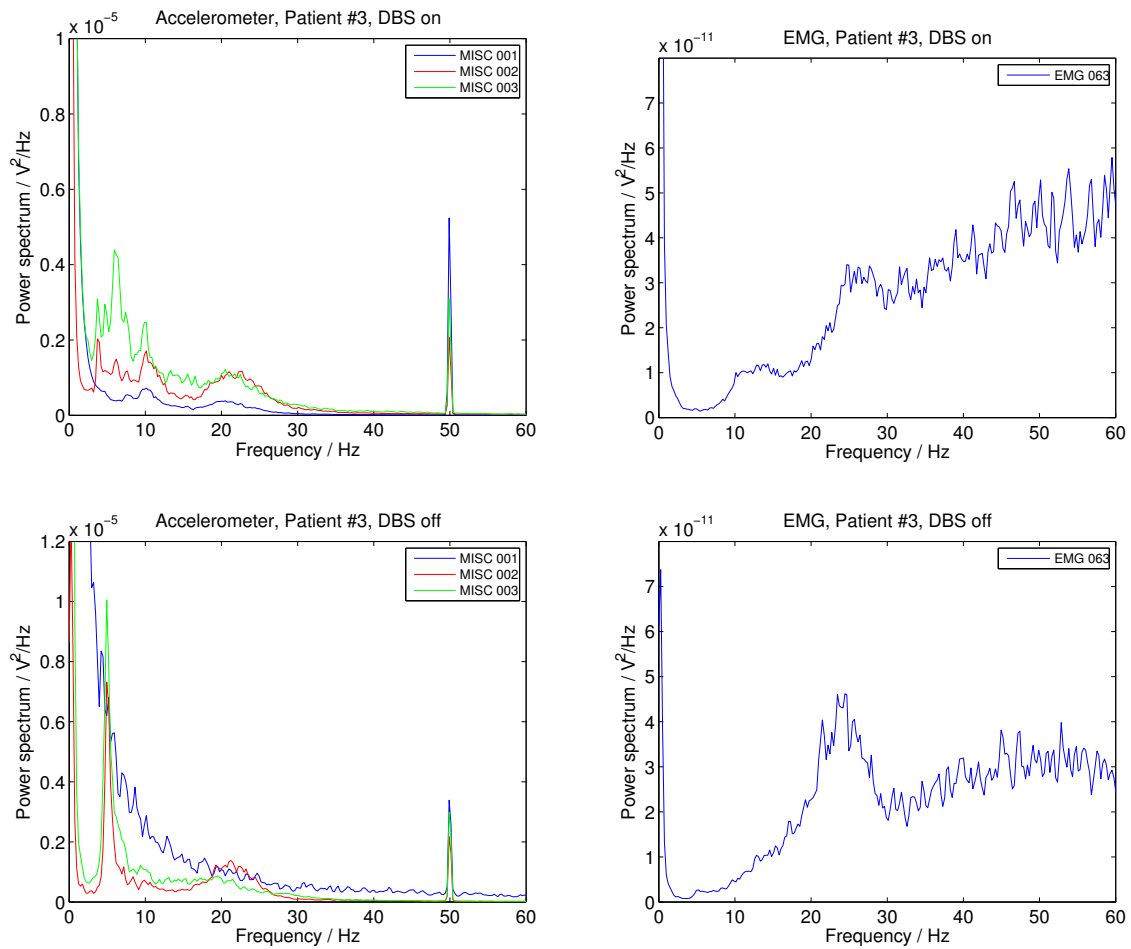


Figure 26: Power spectra: Patient #3.

B Controls: coherence maxima

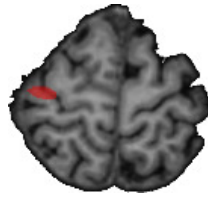
Control #1

right hand: 20-26 Hz

left hand: 21-27 Hz



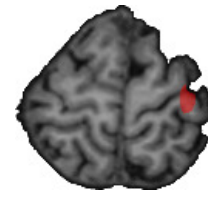
$CKC_{\max} = 0.05$



$CMC_{\max} = 0.04$



$CKC_{\max} = 0.03$



$CMC_{\max} = 0.02$

Control #2

right hand: 19-25 Hz

left hand: 19-25 Hz



$CKC_{\max} = 0.08$



$CMC_{\max} = 0.09$



$CKC_{\max} = 0.06$

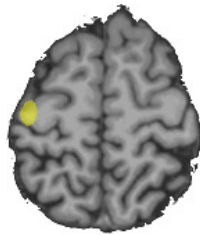


$CMC_{\max} = 0.10$

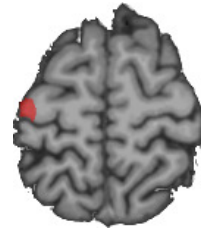
Control #3

right hand: 19-25 Hz

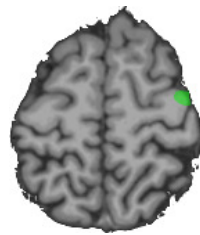
left hand: 18-24 Hz



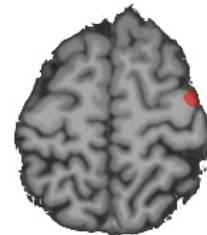
$CKC_{\max} = 0.12$



$CMC_{\max} = 0.10$



$CKC_{\max} = 0.07$



$CMC_{\max} = 0.10$

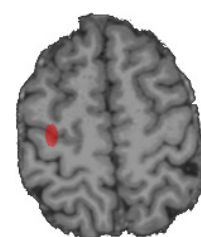
Control #4

right hand: 13-19 Hz

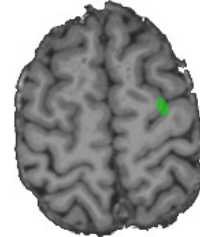
left hand: 18-24 Hz



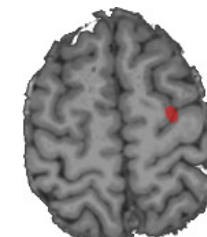
$CKC_{\max} = 0.03$



$CMC_{\max} = 0.03$



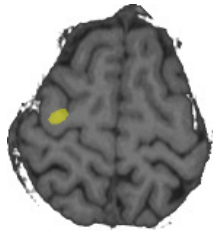
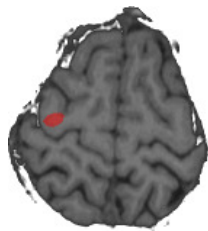
$CKC_{\max} = 0.06$



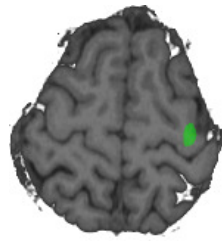
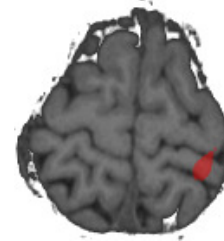
$CMC_{\max} = 0.09$

Control #5

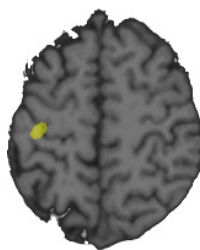
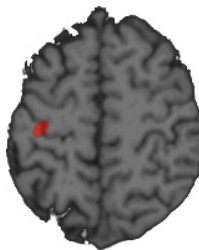
right hand: 22-28 Hz

CKC_{max} = 0.06CMC_{max} = 0.06

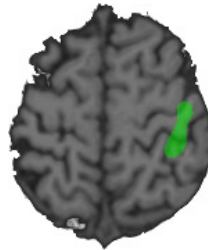
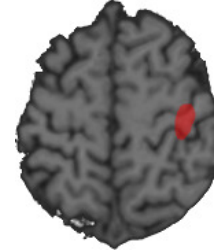
left hand: 20-26 Hz

CKC_{max} = 0.03CMC_{max} = 0.06**Control #6**

right hand: 21-27 Hz

CKC_{max} = 0.06CMC_{max} = 0.03

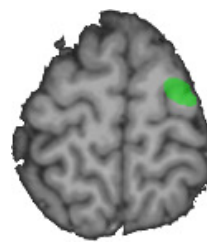
left hand: 19-25 Hz

CKC_{max} = 0.01CMC_{max} = 0.01**Control #7**

right hand: 23-29 Hz

CKC_{max} = 0.01CMC_{max} = 0.02

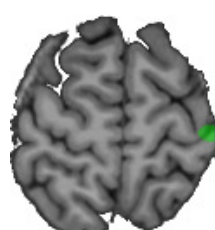
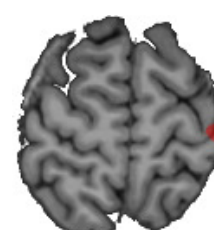
left hand: 24-30 Hz

CKC_{max} = 0.01CMC_{max} = 0.02**Control #8**

right hand: 12-18 Hz

CKC_{max} = 0.01CMC_{max} = 0.01

left hand: 12-18 Hz

CKC_{max} = 0.02CMC_{max} = 0.01

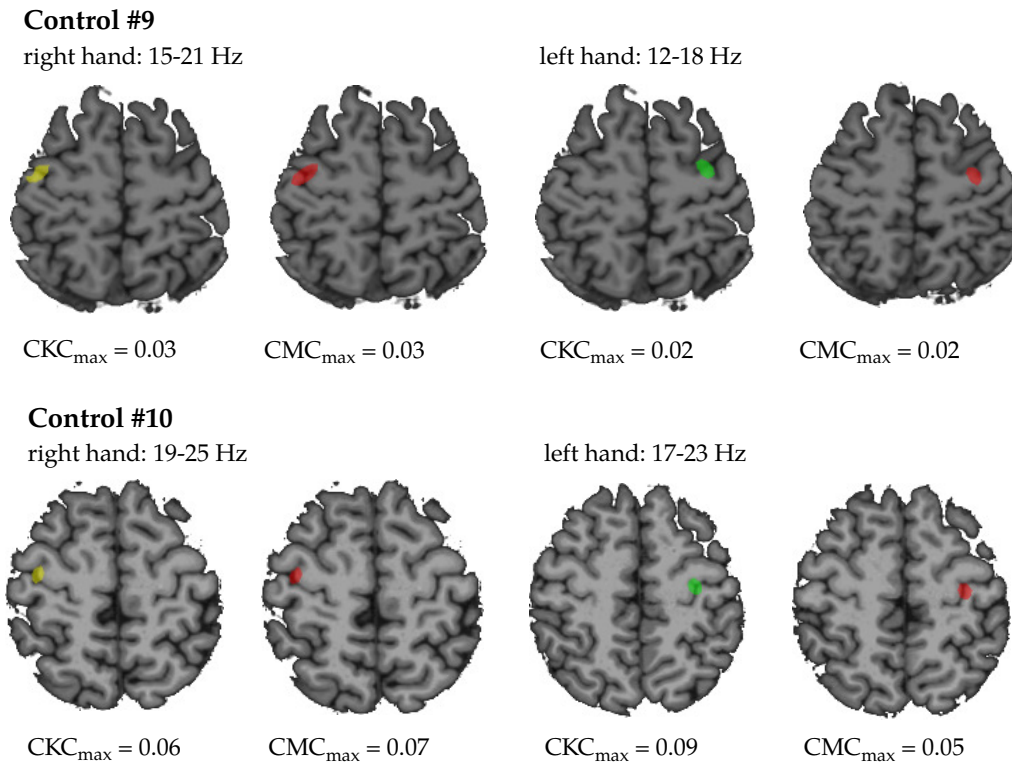


Figure 27: Source-space coherence maxima estimated for the controls. The results are color-coded so that yellow and green mark CKC maxima for the right and the left hand, respectively, and red marks CMC maxima for both hands.